OPTIMIZATION OF SYNTHESIS CONDITIONS OF BORON NITRIDE NANOTUBES (BNNTS) AND THEIR EFFECTS ON EPOXY RESIN CURING

by

YELDA YORULMAZ

Submitted to the Graduate School of Engineering and Natural Sciences

in partial fulfillment of

the requirements for

the degree of Master of Science

Sabancı University

July 2018

OPTIMIZATION OF SYNTHESIS CONDITIONS OF BORON NITRIDE NANOTUBES (BNNTS) AND THEIR EFFECTS ON EPOXY RESIN CURING

APPROVED BY:

Prof. Dr. Melih Papila
(Thesis Supervisor) .....

Prof. Dr. Selmiye Alkan Gürsel .....

Assoc. Prof. Dr. Elif Özden Yenigün .....

DATE OF APPROVAL: 24/07/2018

To my family

Optimization of Synthesis Conditions of Boron Nitride Nanotubes (BNNTs) and Their Effects on Epoxy Resin Curing

Yelda Yorulmaz

Material Science and Engineering

Master of Science Thesis, 2018

Thesis Advisor: Prof.Dr. Melih Papila

Keywords: boron nitride nanotubes, optimization, nanocomposites, cure kinetics, epoxy resin, fast curing

Abstract

Boron nitride nanotubes (BNNTs) are structural analogues of carbon nanotubes (CNTs). The interest in them and their nanocomposites have been growing due to their unique properties. Chemical vapor deposition (CVD) is a relatively cheap and lab scale technique employed in inorganic material synthesis. This thesis work aims to achieve two fundamental goals in two separate chapters.

In the first chapter, the process parameters determining the quality and amount of BNNT synthesis by CVD are evaluated in a response surface methodology framework. A three-level full factorial design where process factors such as reaction temperature, heating rate and reactive gas flow are considered in three levels forming a design space with 27 experiment points. Through a systematic experimentation scheme, three responses determined by sophisticated RAMAN and SEM analysis (namely BNNT diameter, BNNT aspect ratio and wafer coverage) are then fitted into polynomial based surrogate models. Performed ANOVA analyzes suggest that surrogate models are mostly able to predict the change in response with respect to changing process factors. Optimized process conditions aiming to achieve high aspect ratio and high substrate coverage are then presented.

Second part of the thesis focuses on a composite application example of in-house synthesized BNNTs. BNNTs manufactured at the optimized process conditions are introduced to epoxy resin with altering amounts. Specific attention is given to their effect on the curing kinetics of a thermoset system. BNNTs may give alternate fast curing recipes. Through dynamic and isothermal

DSC scans of BNNT/epoxy resin, the curing behavior is firstly studied in detail. Then governing curing mechanism and the effects of BNNT addition is explored by the fitting of appropriate kinetic models onto experimental data.

Bor Nitrür Nanotüplerin (BNNT) Üretim Süreçlerinin Optimizasyonu ve Epoksi Reçine Kürlenmesine Etkileri

Yelda Yorulmaz

Malzeme Bilimi ve Mühendisliği

Yüksek Lisans Tezi, 2018

Tez Danışmanı: Prof.Dr. Melih Papila

Anahtar Kelimeler: bor nitrür nanotüpler, optimizasyon, kür kinetiği, epoksi reçine, hızlı kürlenme

Özet

Bor nitrür nanotüpler (BNNT), karbon nanotüplerin (KNT) yapısal analoglarıdır. BNNT'lerin sahip oldukları yapısal ve fiziksel özelliklere bağlı olarak kendilerine ve oluşturdukları nanokompozitlere gösterilen ilgi artmıştır. Kimyasal buhar biriktirme (KBB) yönteminin, küçük ölçekli inorganik malzeme sentezlerinde kullanılan, nispeten daha uygun bütçeye sahip bir yöntem olduğu bilinmektedir. Bu tez çalışması, iki ayrı bölümde iki temel amacı gerçekleştirmeyi amaçlamaktadır.

Tezin birinci bölümünde, KBB ile BNNT sentezinin kalitesini ve miktarını belirleyen süreç parametreleri tepki yüzey analizi çerçevesinde değerlendirilmiştir. Reaksiyon sıcaklığı, ısıtma hızı ve reaktif gaz akış hızının gibi süreç parametrelerinin BNNT'lerin çap, boy/en oranı ve levha kaplanma oranlarına etkileri 27 farklı noktaya sahip deney uzayında 3 seviyeli tam faktöriyel deneysel tasarım yöntemi kullanılarak incelenmiştir. Sistematik deneylerin sonucunda BNNT çapı, boy/en oranı ve levha kaplanma oranlarındaki değişimler RAMAN ve SEM analizleri ile gözlenmiş ve çok terimli (polinom) vekil modeller geliştirilmiştir. ANOVA analizleri sonucunda, vekil modellerin süreç parametrelerine bağlı olarak sonuçlardaki değişimi tahmin edebildiğini gözlenmiştir. Yüksek boy/en oranına ve levha kaplanma oranına sahip BNNT üretimini hedefleyen koşullar çalışma sonunda sunulmuştur.

Tezin ikinci bölümünde, sentezlenen BNNT'leri içeren kompozit uygulamaları incelenmiştir. Birinci bölümde optimize edilen koşullarda sentezlenen BNNT'ler epoksi reçinelere farklı miktarlarda eklenmiş ve termoset sistemin kür kinetiğine olan etkileri incelenmiştir. BNNT eklenmesinin hızlı kürlenmeye sebep olabileceği düşünülmüştür. Dinamik ve izotermal DSC ölçümleri yapılarak BNNT/epoksi reçine sistemlerin kür davranışları incelenmiştir. Ardından deney sonuçları kullanılarak BNNT'lerin kür mekanizmasına etkileri, kür reaksiyonuna uygun kinetik model ve modele ait katsayılar bulunmuştur.

Acknowledgments

Firstly, I am truly grateful to my supervisor, Prof. Dr. Melih Papila for his guidance, advices and support during both my undergraduate and graduate studies. Being a part of his colorful research group was a beautiful experience.

I would also want to thank to my committee members Prof. Dr. Selmiye Alkan Gürsel and Assoc. Prof. Dr. Elif Özden Yenigün. I am thankful for their fruitful reviews and support on my thesis.

I want to thank Prof. Dr. Yuda Yürüm for allowing me to become a part of this layered project. Also, I would like to thank Prof. Dr. Cleva Ow-Yang, Prof. Dr. Mehmet Ali Gülgün and Prof. Dr. Canan Atılgan for motivating me to become a good material engineer.

My sincere and very special gratitude goes to Dr. Mustafa Baysal and Dr. Kaan Bilge. I was very lucky to be their 'petit'. They taught me, they guided me and they trusted me with their very own project. They always encouraged and supported me even when I did not know I needed the support. They helped me when I felt stuck during my research. I cannot thank them enough for the last three years. It has been a life changing experience for me. They helped me to become a better researcher and more importantly a better person with a wider perspective. I love them both. Moreover, I must thank Melike Mercan Yıldızhan and Güliz İnan Akmehmet for their contributions to this thesis. Also, I would not survive the first year of master without them.

I am happy to thank my colleagues and beautiful research companions in last three years Bengisu Yılmaz, Farzin Javanshour, Onur Zırhlı, and other members of our colorful research group Ayça Ürkmez, Barış Emre Kıral and Farzin Asghari Arpattapeh. Also, I would like to thank my dearest office mates Deniz Anıl and Ayşe Durmuş Sayar. They became very huge parts of my life. I am really going to miss see them every morning. Furthermore, I would like to thank my MatGrad family and friends who made my 8 years in Sabancı very special for me: Tuğçe Akkaş, Senem Seven, Canhan Şen, Oğuzhan Oğuz, Omid Moradi, Emre Burak Boz, Melih Can Taşdelen, Leila Haghighi Poudeh, Burçin Gül, Buket Taş, Erdinç Taş, İpek Bilge, Utku Seven, Onur Özensoy, Efe Armağan, Deniz Köken, Can Akaoğlu, Murat Tansan, Ertunga Eyüboğlu, Aysu Yurduşen and Gökşin Liu. Also, I need to thank Zeynep Boz and Didem Koçhan who were two of the best roommates one can ever ask for and my loveliest friends Ceren Özbay, Burak Ünal, Deniz Sürenkök, Rıdvan Kahraman, Oya Tekbulut, Ömer Mutçalı, Semih Işıklı and Cem Demirgülle.

My beloved, Kerem Kahraman deserves a very special thank you. He always supported, encouraged and motivated me and made me a better person with his endless love. I would not be the same without him.

Also, I would like to thank my aunt Esen, uncle Suat and cousin Ezgi. They never let me feel that my parents were away. They took me as their own and supported me during my studies.

My deepest and sincere thank you goes to my mother Nesrin, father Mustafa and brother Yalın, who have unconditionally loved, supported and guided me. They always respected my decisions and provided everything I needed in my life. I cannot thank and appreciate them enough for everything they have done for me. I am very lucky to be part of this lovely family of ours. I love you all.

Table of Contents

List of Figures

List of Tables

1 Chapter 1

1.1 General Introduction

Boron nitride nanotubes (BNNTs) are structural analogues of carbon nanotubes (CNTs) in which alternating B and N atoms replace C atoms with almost no interatomic space change [1, 2]. BNNTs are theoretically predicted and synthesized in 1995 [3]. Similar to CNTs, BNNTs exhibit superior structural and mechanical properties [4, 5]. In addition, they have higher chemical stability than CNTs [6]. One important difference between these nanotubes is related to their electronic structure. BNNTs are good insulators with a wide band gap (~5.5eV) which is independent from chirality, diameter and number of walls whereas CNTs are conductive materials with a narrow band gap [1, 7, 8]. Due to their similar, unique and superb properties compared to CNTs, BNNTs become a good alternative and the interest in them have been grown recently [1, 4, 9, 10].

Different methods for synthesizing BNNTs have been studied in the literature such as arc discharge[3], laser ablation [11], chemical vapor deposition (CVD) [6, 12, 13], substitution reaction of CNTs [14] or ball milling [15] …etc. Previous studies show that CVD technique is a good candidate for achieving high yield with high quality in relatively lower temperatures and lower costs among the other techniques [4, 9].

Several parameters may affect the yield and properties of BNNTs produced by CVD, such as precursor content, reaction temperature, reactive gas flow rate, heating rate and reaction time [2, 5, 16, 17]. There are previous studies focused on the effects of these parameters on the morphologies of BNNTs [2, 5, 17]. General approach in these studies was changing only one parameter while keeping other parameters constant to understand the effects of the parameter and the procedure was repeated for each parameter consecutively. But this method, which is called as one factor at a time, has some disadvantages. For instance, it neglects the interactions between parameters which may result in inaccurate optimal conditions. Additionally, it requires high number of experiments which increases the time spent and cost [18, 19]. These drawbacks can be eliminated by using another technique called response surface methodology (RSM) which examines the effects of all parameters simultaneously and is a useful method to study interactions of two or more parameters[18].

Optimization of process conditions by using RSM is a well applied method especially in CNT production. Liu et al.[20] employed the RSM methodology to study the effects of reaction temperature, reaction time and reaction gas on synthesis of CNTs. Porro et al. [21] worked on the effects of temperature, carrier gas flow rate, metal catalyst concentration and tilt angle of substrate on the diameter of CNTs. Similarly, Kuo et al.[22] examined the diameter of CNTs as functions of reaction temperature, methane flow rate and chamber pressure by using experimental strategies. Kukovecz et al. [23] studied the effects of reaction temperature, time, preheating time, catalyst mass and flow rate on synthesis conditions of CNTs. See et al.[24] investigated the influence of temperature, deposition time, feedstock concentration and fluidization ratio on CNT formation. Although design of experiment is widely used for CNT production optimization, it is not commonly used in BNNT synthesis even though both have very similar synthesis procedures.

Thermoset polymers are widely used as matrix part of the composite materials [25, 26].Their main difference from thermoplastic polymers is that they experience chemical reactions through their usage while thermoplastics only experience physical changes such as melting [27].Although there are many types of thermoset polymers, epoxy resins have attracted the attention among the other thermoset polymers due to their superior properties such as high modulus, low shrinkage in cure, good adhesion, good chemical and corrosion resistance. Also, the properties of the uncured epoxy resin such as viscosity makes it easy to process and shape. Moreover, their low cost and light weight make them promising materials [26-29]. Due to such interesting properties of epoxy resins, they have a wide range of application areas including high performance composites, electronics, aeronautics …etc. [26, 30-32].

It is known that the curing reaction of epoxy resin is an important factor for the properties of the final product. Linear epoxy monomers are linking to each other to form a three-dimensional crosslinked network during the curing process in which viscosity of the thermosets increases and cause a decrease in mobility of polymer chains. At the end of the process, they become rigid materials [27, 33]. Another effecting factor on the properties of the final product is the addition of filler materials. This approach enables to tune the final properties of polymer nanocomposites such as enhanced mechanical and physical properties Usually, many thermosets are used in reinforced or filled form to tune their physical properties or to reduce their costs [27, 34].

Since the discovery of nanotube structures in 1991 [35], the interest in nanotube/polymer nanocomposites has increased and created a new class of reinforced materials [31]. More specifically, the studies about improving the various properties of epoxy resins by adding nanotubes have been widely performed [31, 33, 36, 37]. Most of the initial studies were performed by using carbon nanotubes (CNTs) due to their impressive properties such as high aspect ratio, good thermal and electrical conductivity and superior mechanical properties [32, 36, 38]. Another promising alternative to prepare such nanotube/epoxy resin nanocomposites is boron nitride nanotubes (BNNTs). Addition to superior physical and structural properties of BNNTs, alternating B and N atoms in the structure with different affinities result in polarization of B-N bond which may offer an advantage for better compatibility. In other words, BNNTs are expected have superior binding interfaces due to their polarized structures compared to CNTs [39].

As mentioned before, nanofillers are widely used reinforcement agents for polymer composites. Idea of mechanically strong, thermally enhanced, electrically insulator, transparent or whitish and lightweight composites makes BNNTs good candidates as nanofillers. Although there are few studies for the different thermal and mechanical properties of BNNT/epoxy nanocomposites [40, 41], there is not a well-established study related to the effects of BNNTs on the curing mechanisms of epoxy resins which is very crucial for composite processing. But on the other hand, there are well established studies for the curing mechanisms of different types of CNT/epoxy resin nanocomposites. Zhou et al.[33] suggested that addition of multi walled CNTs to epoxy imidazole system created an acceleration effect on the overall curing. Puglia et al.[36] demonstrated that single wall CNTs incorporated into diglycidyl ether of bisphenol A-based (DGEBA) epoxy resin acted as a strong catalyst for curing system. Xie at al. [32] studied the effects of addition of multi wall CNTs into tetraglycidyl-4,4’-diaminodiphenylmethane /4,4-diaminodiphenylsulfone (TGDDM/DDS) system which showed that CNTs had an acceleration effect on the cure reaction.

Therefore, the main focus of this study is to optimize the synthesis conditions of boron nitride nanotubes (BNNTs) and investigate the effects of BNNTs synthesized under these optimum conditions on cure mechanism of widely used epoxy resin systems.

2 Chapter 2: Optimization of Synthesis Conditions of Boron Nitride Nanotubes (BNNTs) by Chemical Vapor Deposition (CVD)

2.1 Introduction

Boron nitride nanotubes (BNNTs) are structural analogues of carbon nanotubes (CNTs) in which alternating B and N atoms replace C atoms with almost no interatomic space change [1, 2]. BNNTs are theoretically predicted and synthesized in 1995 [3]. Similar to CNTs, BNNTs exhibit superior structural and mechanical properties [4, 5]. In addition, they have higher chemical stability than CNTs [6]. One important difference between these nanotubes is related to their electronic structure. BNNTs are good insulators with a wide band gap (~5.5 eV) which is independent from chirality, diameter and number of walls whereas CNTs are conductive materials with a narrow band gap [1, 7, 8]. Due to their similar, unique and superb properties compared to CNTs, BNNTs become a good alternative and the interest in them have been grown recently [1, 4, 9, 10].

Different methods for synthesizing BNNTs have been studied in the literature such as arc discharge[3], laser ablation [11], chemical vapor deposition (CVD) [6, 12, 13], substitution reaction of CNTs [14] or ball milling [15] …etc. Previous studies show that CVD technique is a good candidate for achieving high yield with high quality in relatively lower temperatures and lower costs among the other techniques [4, 9].

Several parameters may affect the yield and properties of BNNTs produced by CVD, such as precursor content, reaction temperature, reactive gas flow rate, heating rate and reaction time [2, 5, 16, 17]. There are previous studies focused on the effects of these parameters on the morphologies of BNNTs [2, 5, 17]. General approach in these studies was changing only one parameter while keeping other parameters constant to understand the effects of the parameter and the procedure was repeated for each parameter consecutively. But this method, which is called as one factor at a time, has some disadvantages. For instance, it neglects the interactions between parameters which may result in inaccurate optimal conditions. Additionally, it requires high number of experiments which increases the time spent and cost [18, 19]. These drawbacks can be eliminated by using another technique called response surface methodology (RSM) which examines the effects of all parameters simultaneously and is a useful method to study interactions of two or more parameters[18].

Optimization of process conditions by using RSM is a well applied method especially in CNT production. Liu et al.[20] employed the RSM methodology to study the effects of reaction temperature, reaction time and reaction gas on synthesis of CNTs. Porro et al. [21] worked on the effects of temperature, carrier gas flow rate, metal catalyst concentration and tilt angle of substrate on the diameter of CNTs. Similarly, Kuo et al.[22] examined the diameter of CNTs as functions of reaction temperature, methane flow rate and chamber pressure by using experimental strategies. Kukovecz et al. [23] studied the effects of reaction temperature, time, preheating time, catalyst mass and flow rate on synthesis conditions of CNTs. See et al.[24] investigated the influence of temperature, deposition time, feedstock concentration and fluidization ratio on CNT formation. Although design of experiment is widely used for CNT production optimization, it is not commonly used in BNNT synthesis even though both have very similar synthesis procedures.

Therefore, the main focus of this chapter is to apply RSM method to optimize synthesis conditions of BNNTs by CVD. For this purpose, reaction temperature, reactive gas flow rate and heating rate were chosen as process parameters and diameter, aspect ratio and wafer coverage of the nanotubes as the responses of interest. Empirical models were developed to correlate parameters to responses.

2.2 Approach

2.2.1.1 Definition of Experiment/Run

In this study, every different set of synthesis conditions of BNNTs refers to an experiment/run. The conditions were defined as functions of reaction temperature, heating rate and reactive gas flow rate.

2.2.1.2 Response Surface Methodology (RSM)

Response surface methodology is a collection of statistical techniques to represent the experimental data as a mathematical approximation model. The model or response surface approximation can help to predict the output(s) of interest at the conditions for which the experimental data is not available [18].One of the advantages of RSM is that it can reveal the interactions between parameter effects which is crucial while seeking an optimum solution. Also,

it typically requires lower number of experiments compared to one factor at a time method [18, 20] when global optimal setting is aimed.

Three parameters were chosen for this study: reaction temperature (X_1), heating rate (X_2) and reactive gas flow rate (X_3) each with three different levels to consider in the experimental design [19]. The number of required experiments, N, for a full factorial design of three levels is calculated as $N=3^k$ where k is the number of factors [18]. Therefore, $N=3^3=27$ experiments (see Figure 1) were performed during this study to understand effects of chosen parameters on the diameter (Y_1), aspect ratio (defined as thickness/diameter) (Y_2) and wafer coverage ratio (Y_3) of the nanotubes.

The coding of the factors is typically implemented for systematic optimization studies which is a conversion of real values into dimensionless coordinates [19]. The related conversion can be performed by following the Equation 1 where X_i represents the coded variable whereas v_i is the value of the parameter within the range of max and min v_i. Thus, the levels of each factor were coded as '-1, 0, +1' corresponding to the lowest, middle and the highest values of each parameter, respectively (Table 1).

$$X_i = \frac{v_i - [(maxv_i + minv_i)/2]}{[(maxv_i - minv_i)/2]} \quad (1)$$

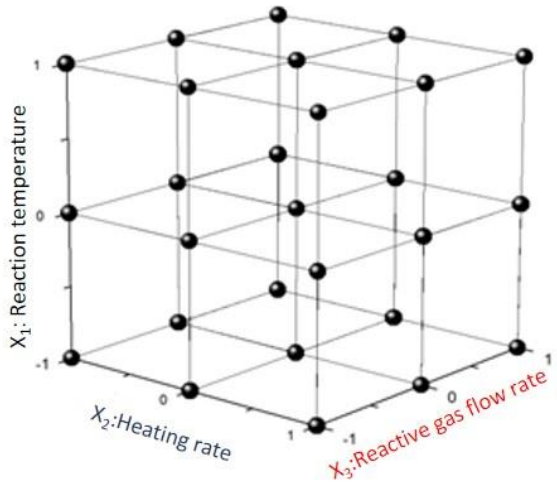

Figure 1:3^3 factorial experimental design

Table 1:Experimental Ranges and Coded Variables for BNNT Synthesis

Parameters\ Coded Variables	-1 (The Lowest)	0 (Middle)	1 (The Highest)
X_1: Reaction Temperature (˚C)	1000	1100	1200
X_2: Heating Rate (˚C/min)	5	10	15
X_3: NH_3 flow rate (ml/min)	100	150	200

Seeking empirical models to understand the relation between parameters and system responses in optimization studies [18], quadratic polynomial equations for each response were developed in this study as given below (Eq 2),

$$\hat{Y} = b_1 + b_2x_1 + b_3x_2+b_4x_3+ b_5x_1x_2+b_6x_1x_3+b_7x_2x_3+b_8x_1^2+b_9x_2^2+b_{10}x_3^2 \quad (2)$$

where $\hat{Y}$ and b_i represent predicted response and coefficients, respectively.

Addition to individual response analyzes, optimization study incorporating multi responses was conducted. When there are more than one response of interest, a favorable degree of compliance with each response/target is sought simultaneously for overall performance [18]. In other words, a compromised solution must be found [42]. For this purpose, aspect ratio and wafer coverage were chosen as multiple responses, considering diameter was included in the aspect ratio.

DESIGN EXPERT software was used for regression analyzes to fit the predicted equations and for statistical analyzes.

2.3 Experimental Procedure and Characterization

2.3.1.1 Synthesis of Boron Nitride Nanotubes (BNNTs) by Chemical Vapor Deposition

Boron nitride nanotubes (BNNTs) were synthesized by following the chemical vapor deposition (CVD) method. Two quartz tubes were placed inside each other with the diameters of 60 mm and 20 mm in a horizontal furnace. The inner tube was chosen as a closed end type to trap vapor for further growth and it was placed in opposite direction of the reactive gas flow (Figure 2). Precursor material was prepared by mechanical grinding of amorphous B, MgO and Fe_2O_3 powders in

specific molar ratios. Si wafer coated with Al_2O_3 which works as a buffer layer and MgO which works as the catalyst by thermal evaporation. The precursor material was put inside an alumina crucible and the top of the crucible was covered by the Si wafer. Then, the crucible was placed inside the inner tube and the tube was placed inside furnace (Figure 3). Then, the air inside the tube was evacuated by vacuum pump. After the evacuation, furnace was heated with the chosen heating rate to the required reaction temperature under the chosen NH_3 flow rate. [16, 17]

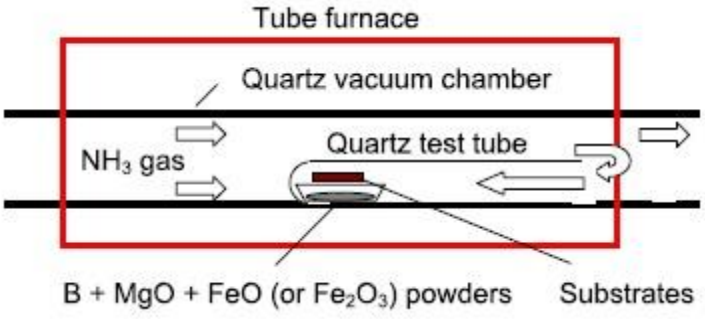

Figure 2: Schematic of Vapor Trapped Chemical Vapor Deposition (CVD) [16]

Figure 3:Furnace system used for the synthesis of BNNTs

Vapor–liquid–solid (VLS) mechanism suggests that the partially melted catalysts creates a vapor pressure. When the pressure reaches the critical point, vapor condenses on the top of the substrate.

The as-formed BN particles diffuse into the condensed catalyst particles. Then, they start to agglomerate and form one dimensional nanotube structures when they supersaturate [2, 43].

$$2MgO(s) + 2B(s) \rightarrow B_2O_2(g) + 2Mg(g)$$

$$2FeO(s) + 2B(s) \rightarrow B_2O_2(g) + 2Fe\ (s)$$

$$B_2O_2(g) + 2NH_3(g) \rightarrow 2BN(nanotube) + 2H_2O(g) + H_2(g)$$

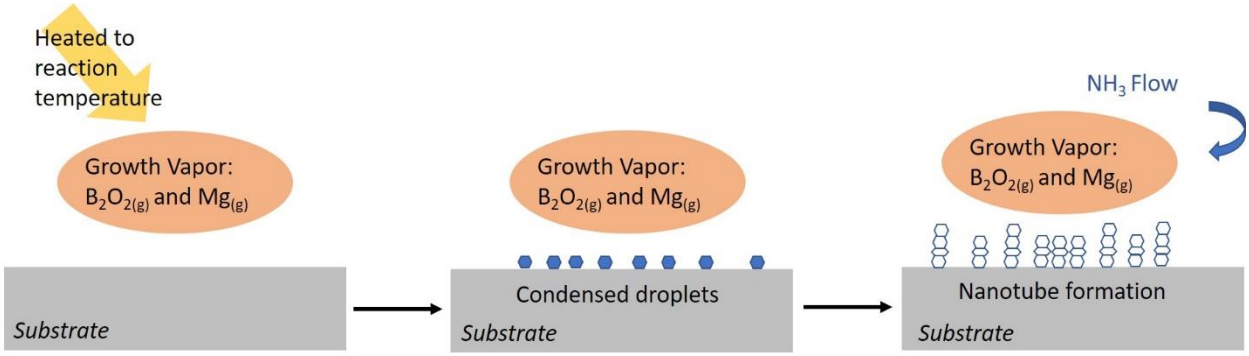

Figure 4:Illustration of V-L-S mechanism

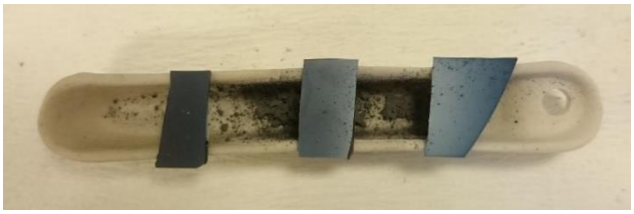

Figure 5:Image of grown BNNTs on top of Si wafer

2.3.1.2 Si Wafer Coating

The properties of substrate are directly related to the growth and the quality of BNNTs produced by CVD. In other words, the coating of Si wafers is essential to control the growth and the increase the quality of nanotubes. Literature review shows that MgO is one of the best resulting catalyst for the CVD growth of BNNTs[44] . Thus, Si wafers were decided to be coated by the catalyst MgO. Also, Al_2O_3 was chosen to be a buffer layer to work as diffusion barrier between MgO and Si to minimize their interactions which reduces the activity of catalyst. All of the coating works were performed in the clean room by using Torr e-beam and Thermal Evaporator under the 10^{-6} Torr vacuum environment. The average thicknesses of Al_2O_3 layers which was coated by e-beam were

measured as 20-30 nm while the average thicknesses of MgO layers which was coated by thermal evaporation were measured as 30 nm.

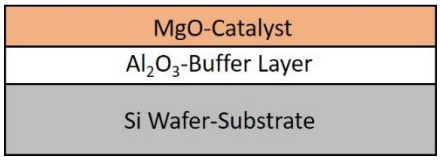

Figure 6:Illustration of coated Si substrate

2.3.1.3 Growth Time of BNNTs at the Reaction Temperature

Another factor which affects the BNNT production is growth time. The waiting time at the reaction temperature is a governing factor on the amount and morphology of final BNNT products. In order to the optimize the process, two different growth times were chosen as 30 minutes and 1 hour. The SEM images showed that longer growth time results in longer but entangled nanotube structures (Figure 7). Thus, growth time was chosen as 30 minutes for the optimization study to ease further analyzes.

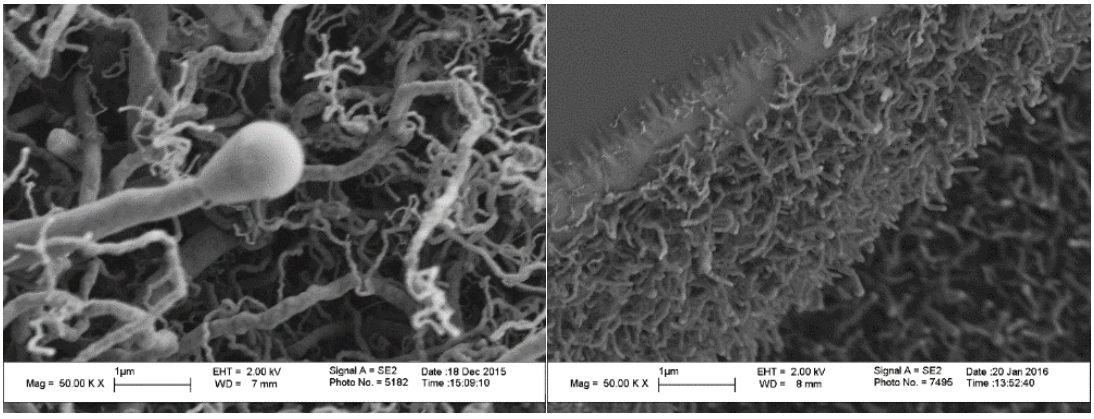

Figure 7:SEM images of BNNTs for different growth time at the reaction temperature a)1-hour b)30 minutes

2.3.1.4 Molar Ratio of Precursor Materials

Another factor affecting the production of BNNTs is molar ratio of the precursor material's compounds. Synthesis of BNNTs by CVD method requires the formation of B_2O_2 as an intermediate phase which is a result of the interaction between B and O. Thus, in order to get better

control of the results, different stochiometric ratios were investigated for the preparation of precursor material. The candidate molar ratios of B, MgO and Fe_2O_3 were chosen as 4:1:1 and 2:1:1, respectively. The experimental conditions were kept the same to examine the effects of two different molar ratios on the growth of nanotubes (reaction temperature, heating rate, NH_3 flow rate were 1100˚C, 10˚C/min and 200 ml/min, respectively). It was clear that molar ratio of 4:1:1 gave longer and thinner nanotubes when the morphologies of produced BNNT were examined (Figure 8). Thus, molar ratio of 4:1:1 was chosen for further studies.

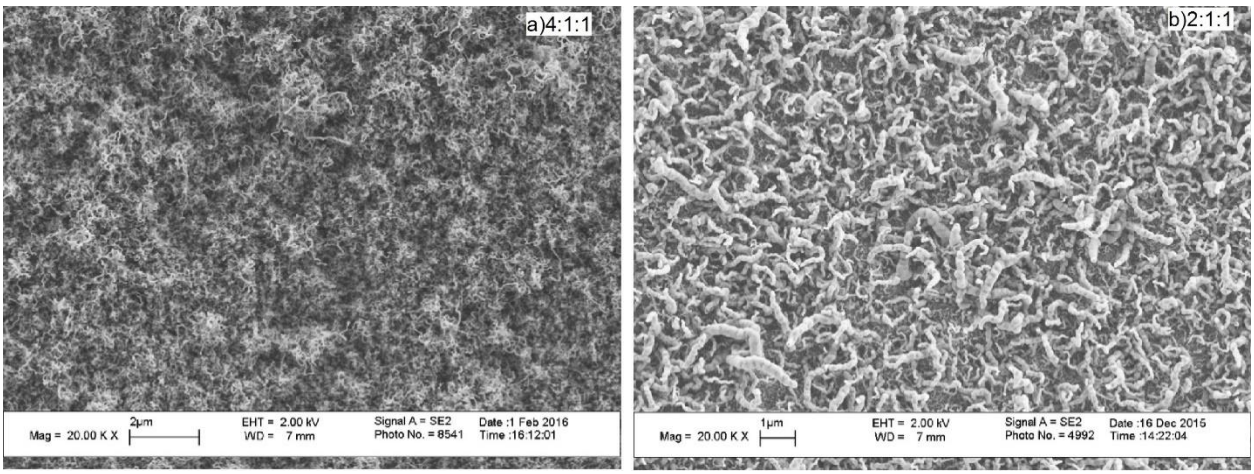

Figure 8:SEM images of BNNTs with different precursor molar ratios a) 4:1:1 b) 2:1:1

2.3.1.5 Preliminary Characterizations of Synthesized BNNTs

2.3.1.6 UV-VIS Spectroscopy

It is known that the BNNTs are good insulators with a wide band gap (~5.5 eV) which is independent from chirality, diameter and number of walls [1, 7, 8]. Thus, UV-VIS spectroscopy was used to calculate the band gap of the synthesized BNNTs as an easy and fast characterization for understanding whether the nanotubes were successfully produced. BNNTs were synthesized at three different reaction temperatures, 1000˚C, 1100˚C and 1200˚C, while 200 ml/min NH_3 flow rate and 10˚C /min heating rate were kept constant. Each wafer was sonicated in the ethanol to separate BNNTs from the surface of wafers. Then, the solutions were placed into quartz cuvettes. UV-VIS measurements were performed by using Shimadzu 3150 UV-VIS Spectrophotometer between 200-800 nm. According to the results, band gaps for each sample were calculated approximately 5.8 eV which agree with the literature (Figure 9).

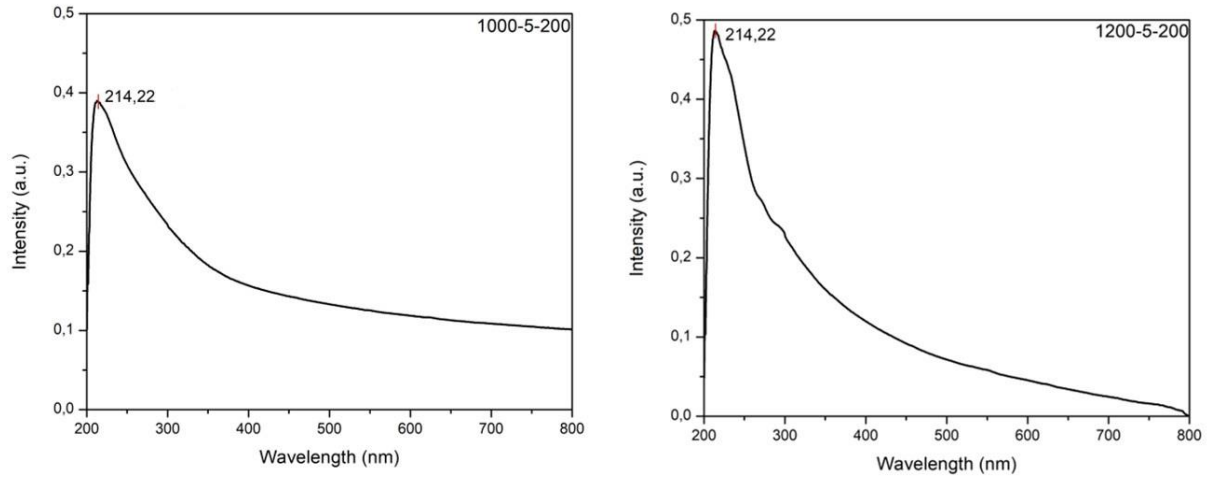

Figure 9:UV-VIS graphs of two different experimental point at 1000˚C (left) and 1200˚C (right)

2.3.1.7 Transmission Electron Microscopy (TEM)

Additional characterization of the produced BNNTs were performed by transmission electron microscopy (TEM) and electron energy loss spectroscopy (EELS). Cs-corrected JEOL ARM 200 Cold FEG TEM was used for structural analysis. Gatan-GIF Quantum ER Spectrometer was used for elemental analysis.

As a first way for the TEM sample preparation, the produced BNNTs were scratched from on top of the Si wafer and mechanically grinded with the ethanol medium. TEM micrographs showed that BNNTs stayed in agglomerated form (Figure 10) which made length measurements not possible. As a second way, sonication was used for collecting BNNTs on top of Si wafer. Wafer and ethanol were sonicated for 90 minutes. After the sonication, the transparent color of ethanol turned into whitish color which indicated that the BNNTs were separated from the wafer and dispersed in ethanol. TEM micrographs showed that this method was successful and prevented agglomeration (Figure 11). Thus, specimen via sonication was used for further TEM analyzes.

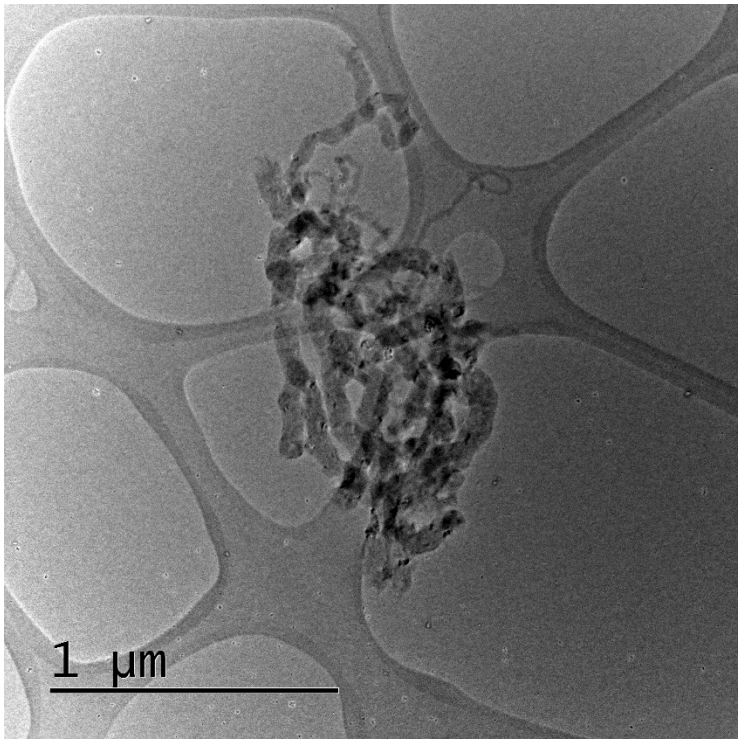

Figure 10:Micrograph of agglomerated BNNTs obtained by mechanical scratching

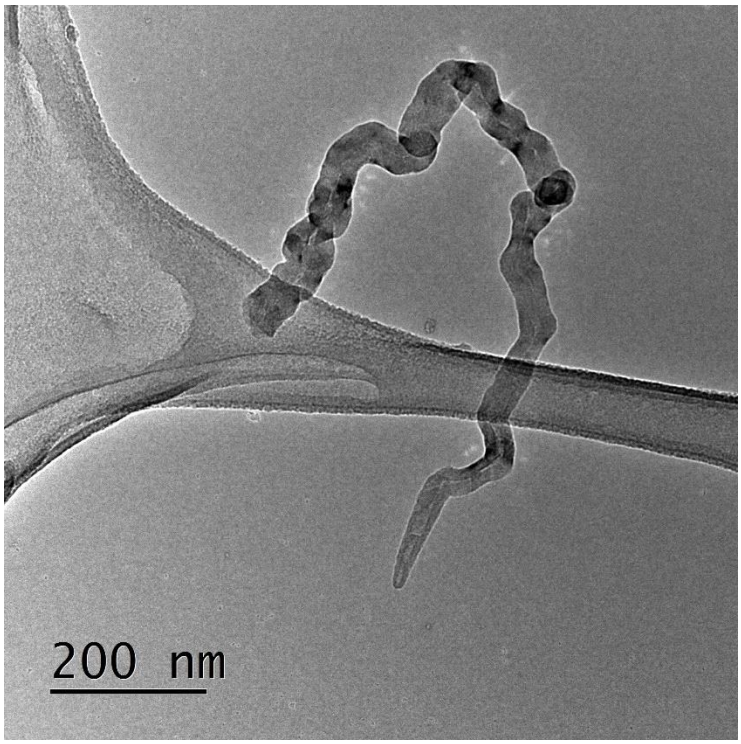

Figure 11:Micrograph of BNNTs obtained by sonication

The results of High Resolution TEM (HRTEM) analysis proved that the multiwalled BNNTs were successfully produced (Figure 12 a). The interatomic distance (interplanar spacing) of BNNTs were measured 0.32 nm in accordance with the literature (Figure 12 b) [45]. Addition to interatomic space distance, average diameter and length values of the nanotube in Figure 11 were measured to have an initial information about the scale of nanotubes. 20 different measurements were performed by using Image J and average diameter was measured as 35.47 nm with a standard deviation of 11 nm whereas average length was measured as 1259.2 nm with a standard deviation of 36.38 nm.

EELS analysis was performed by Scanning transmission electron microscopy (STEM) mode for elemental analysis and 0.25 eV dispersion value was chosen to observe both B and N K-edges. The observed spectrum showed the characteristic K-edge peaks of both B and N at 188 and 401 eV, respectively (Figure 13).

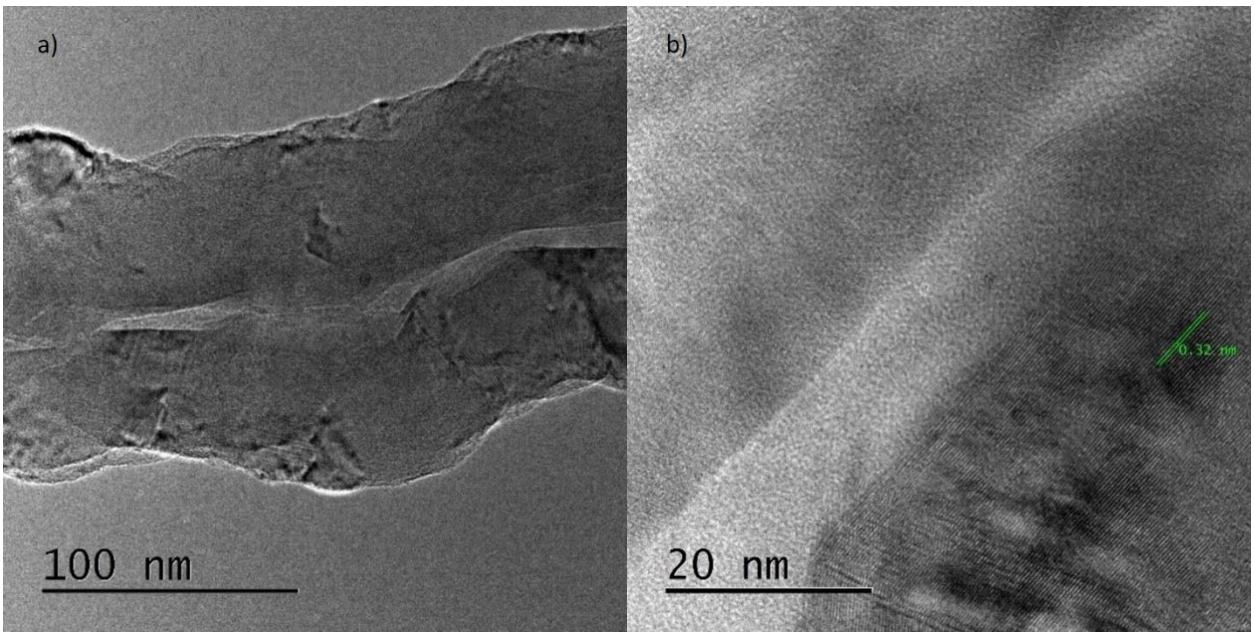

Figure 12: a) Wall structure of BNNTs synthesized at 1100˚C, 10˚C/min heating rate and 200 ml/min NH_3 flow rate b) Interatomic space distance

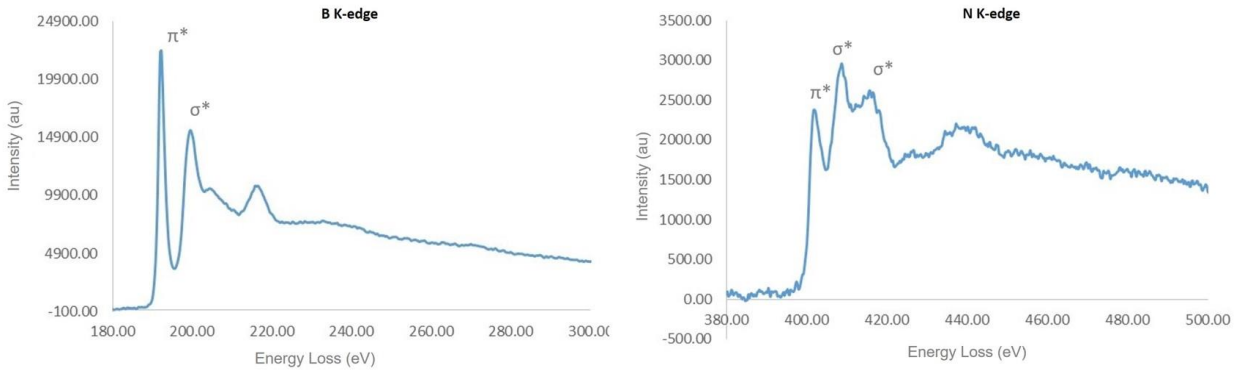

Figure 13:B and N K-edges of BNNTs obtained by EELS

2.3.1.8 Scanning Electron Microscopy (SEM)

SEM images of the produced BNNTs were taken with LEO Supra VP35 field emission scanning electron microscope. Images of each experiment at 50K magnification were used for diameter analysis. Diameter of 100 different tubes were measured for each sample by using Image J software. Average diameter and standard deviation of the nanotubes were calculated according to the measurement results.

2.3.1.9 Raman Spectroscopy

It is a known that the BNNTs have a characteristic Raman shift around 1365 cm^{-1} and Raman spectroscopy is a widely used analysis technique for BNNTs [5, 16, 46]. The shift is attributed to E_{2g} mode of vibrations. In other words, B and N atoms move against each other within the plane and cause high frequency counter phase vibrations [16, 17, 46].

The Raman scattering experiments were performed with Renishaw inVia Reflex Microscope and Spectrometer, equipped with 532 nm visible green laser at room temperature in ambient environment. The calibration of the instrument was done with a silicon wafer by obtaining pure Si signal at ~520 cm^{-1}. Raman spectra of the samples were obtained between 100 cm^{-1} and 3000 cm^{-1} with 5% of the laser beam power and an exposure time of 10 seconds at 50x magnification. Spectral analyses were performed with the Renishaw WiRE software.

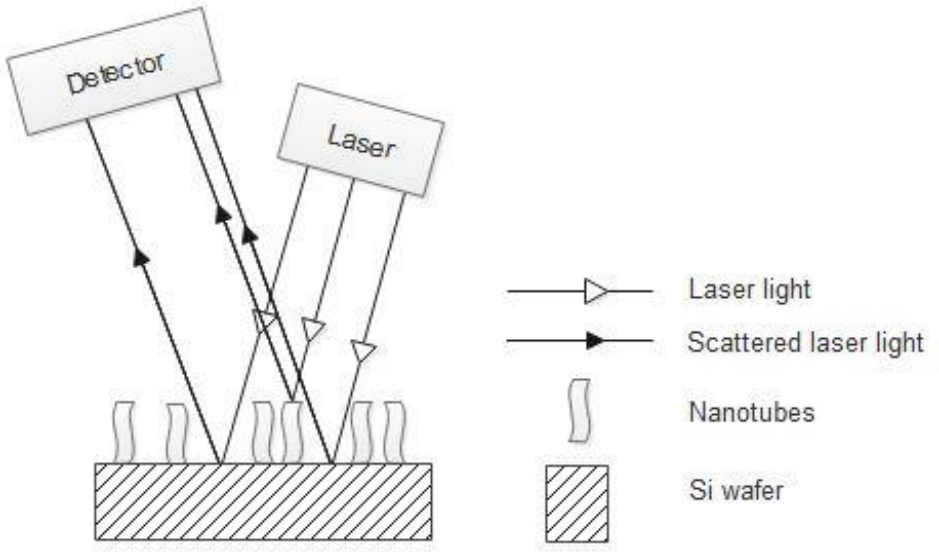

Figure 14:Illustration of Raman spectroscopy measurements of BNNTs on Si wafer

The obtained Raman spectra of the all samples showed two distinct peaks: the first one is around 1365 cm^{-1} and belongs to BNNTs as shown in the literature before [5, 16, 46]. The second one is around 520 cm^{-1} and comes from the Si wafer [47]. As illustrated in Figure 14, some of the incident beam scatters from BNNTs while some of them passes through the BNNTs and reaches to Si wafer below the tubes.

The Raman peak intensity is related to concentration of species [48], but it may also vary with the laser power (Figure 15). To avoid the effect of laser power, all measurements were performed at constant laser power of 5%. Yet, the intensity may still be affected by the instrumental conditions. Since the Si wafer has the same properties for each sample, taking the ratio between intensities of BNNT peak and Si peak allows to comment on the relative concentrations by minimizing the instrumental effects [47, 48]. The ratio of the intensities of the BN peak to Si peak was considered as a measure for wafer coverage by the BNNTs. To circumvent errors due to concentration differences on top of the wafer surface, measurements were performed from 20 different points which were chosen homogenously with the help of a MATLAB algorithm for each sample and then the calculations were made (Figure 16).

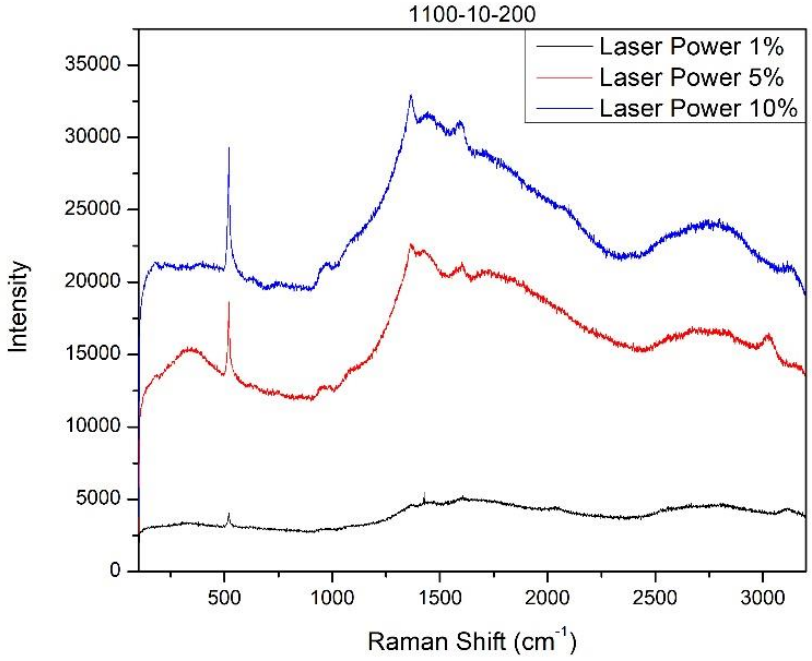

Figure 15: Raman spectra of the same sample with different laser powers

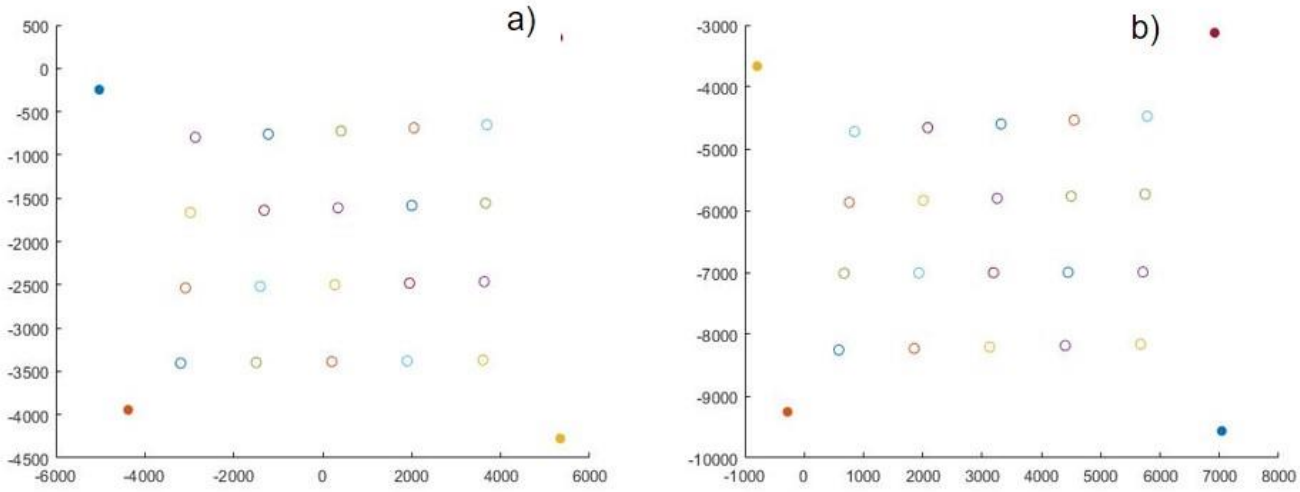

Figure 16:20 points simulations for MATLAB a)1000-10-150 b)1000-10-200

The curly and entangled morphology of BNNTs made individual length measurements of nanotubes difficult by microscopic techniques but at the same time it caused a film formation on top of Si wafer. Therefore, Raman spectroscopy measurements were used to calculate BNNT film thickness. Although the exact length of the produced BNNTs cannot be found by this technique, the thickness of BNNT formation on top of the surface can be found. Determination of film thickness of metal oxide systems is a previously used technique in the literature [49]. The transmitted light coming from the two parallel surfaces (wafer surface and nanotube surface) forms interferences due to phase differences. The frequency of these is related to the film thickness which is called as Fabry-Perot resonance (Eq 3).

$$d = \frac{m}{2n(v_2 - v_1)} \tag{3}$$

where d is film thickness, m is number of minimums between two interferences, n is the refractive index of the material and $v_2 - v_1$ is the difference between the wavenumber of the highest and the lowest interferences. The refractive index of metal oxide coating on top of the Si wafer was neglected since it was very thin (~30 nm). Generally, three different interferences were observed in Raman spectra. These inferences were fitted to calculated film thicknesses. To increase the reliability of the results, average value of 20 different measurements from the wafer was used. Figure 17 shows the example fit for the study.

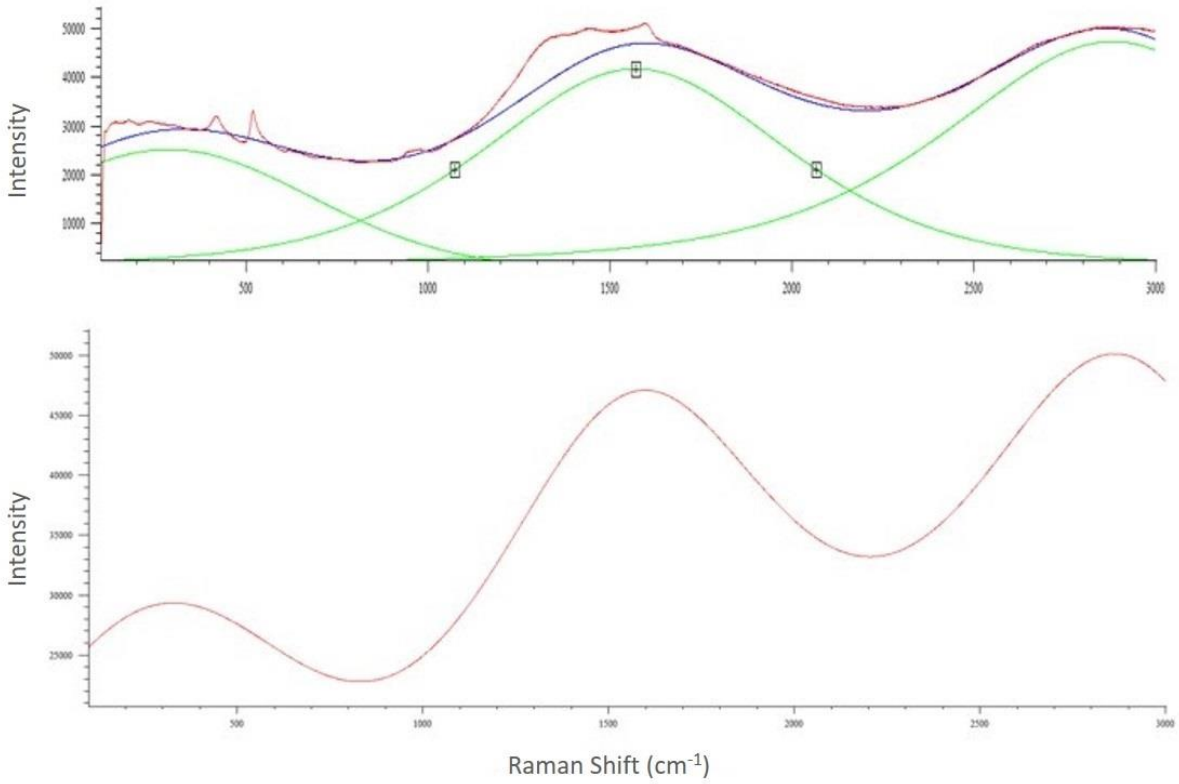

Figure 17: Example fit for 1200-5-150

Note that there is a correlation between the length of BNNT and the thickness, i.e. the short nanotubes result in thinner films whereas longer and curly nanotubes result in thicker films which were used for aspect ratio calculations. Thus, errors in aspect ratio was minimized. Moreover, coverage of nanotubes was examined as well since the actual length of nanotubes were not calculated.

2.4 Results and Discussion

2.4.1.1 Characterization Results

2.4.1.2 SEM Results

The SEM images of the BNNTs produced under 200, 150 and 100 ml/min NH_3 flow rate are shown in Figures 18,19 and 20. The different morphologies were observed by the SEM images. Average diameter and standard deviation measurements were performed from 100 different tubes by using Image J software (Table 2).

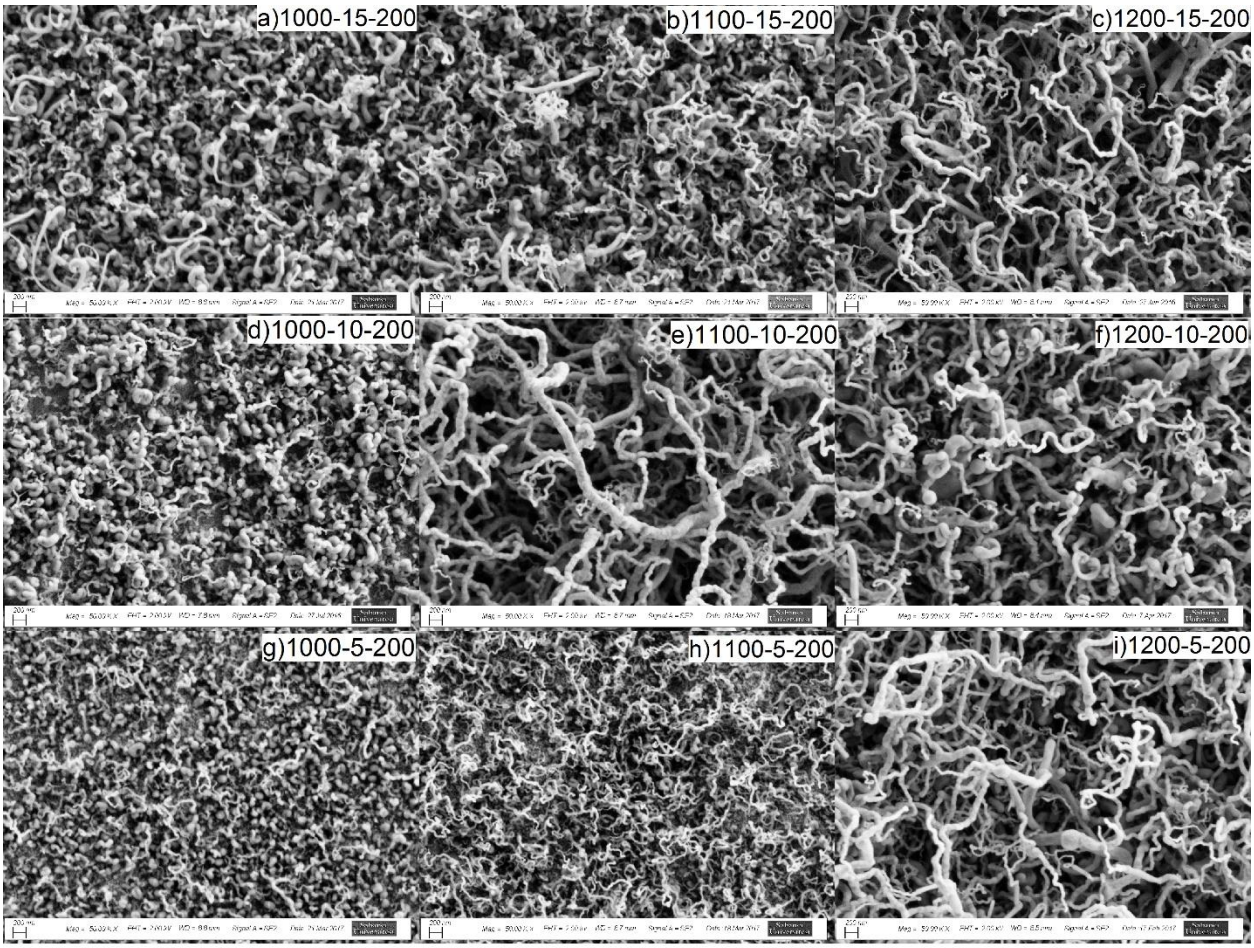

Figure 18:SEM images of BNNTs produced under 200 ml/min NH_3 flow rate (Right top: Experimental point)

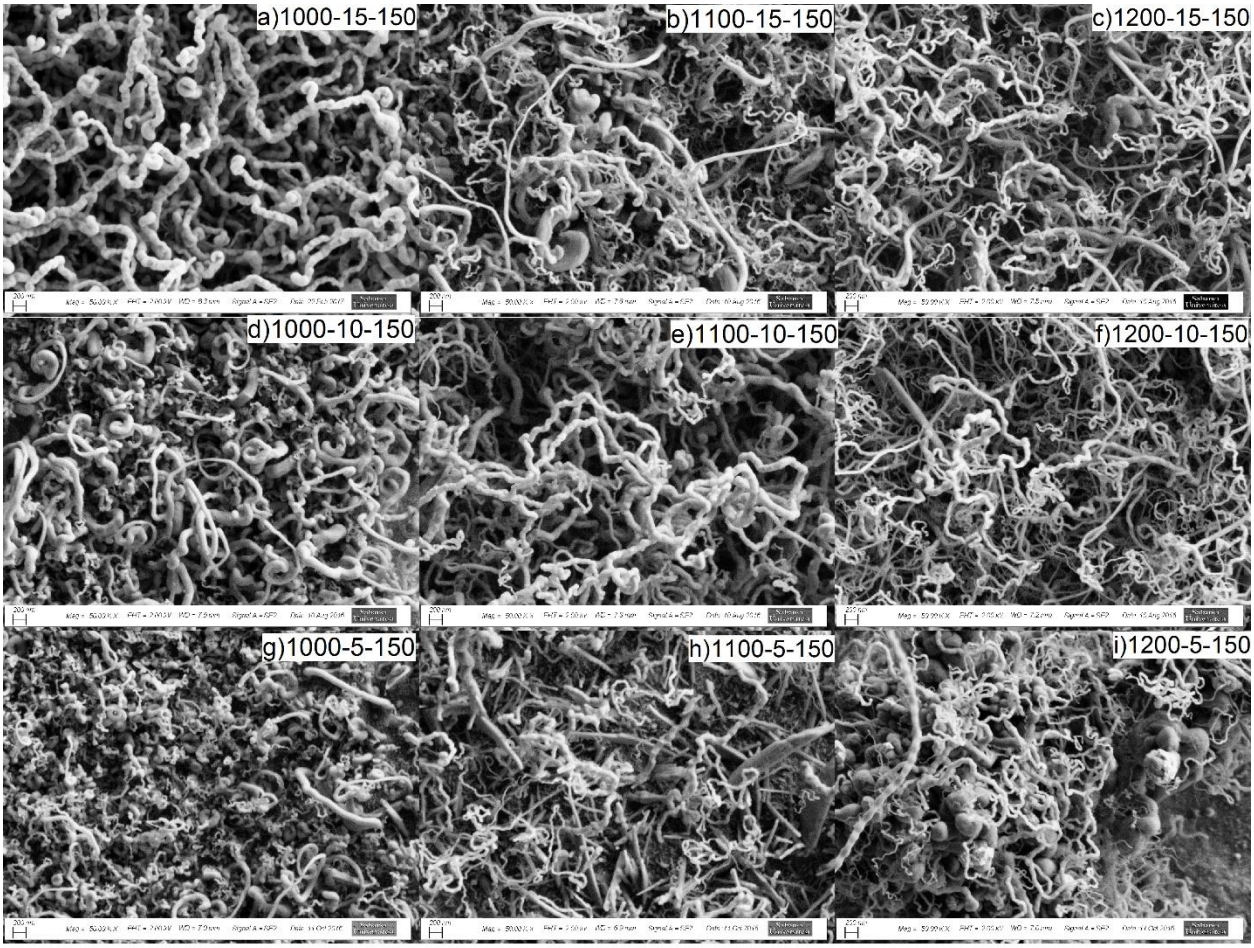

Figure 19: SEM images of BNNTs produced under 150 ml/min NH_3 flow rate (Right top: Experimental point)

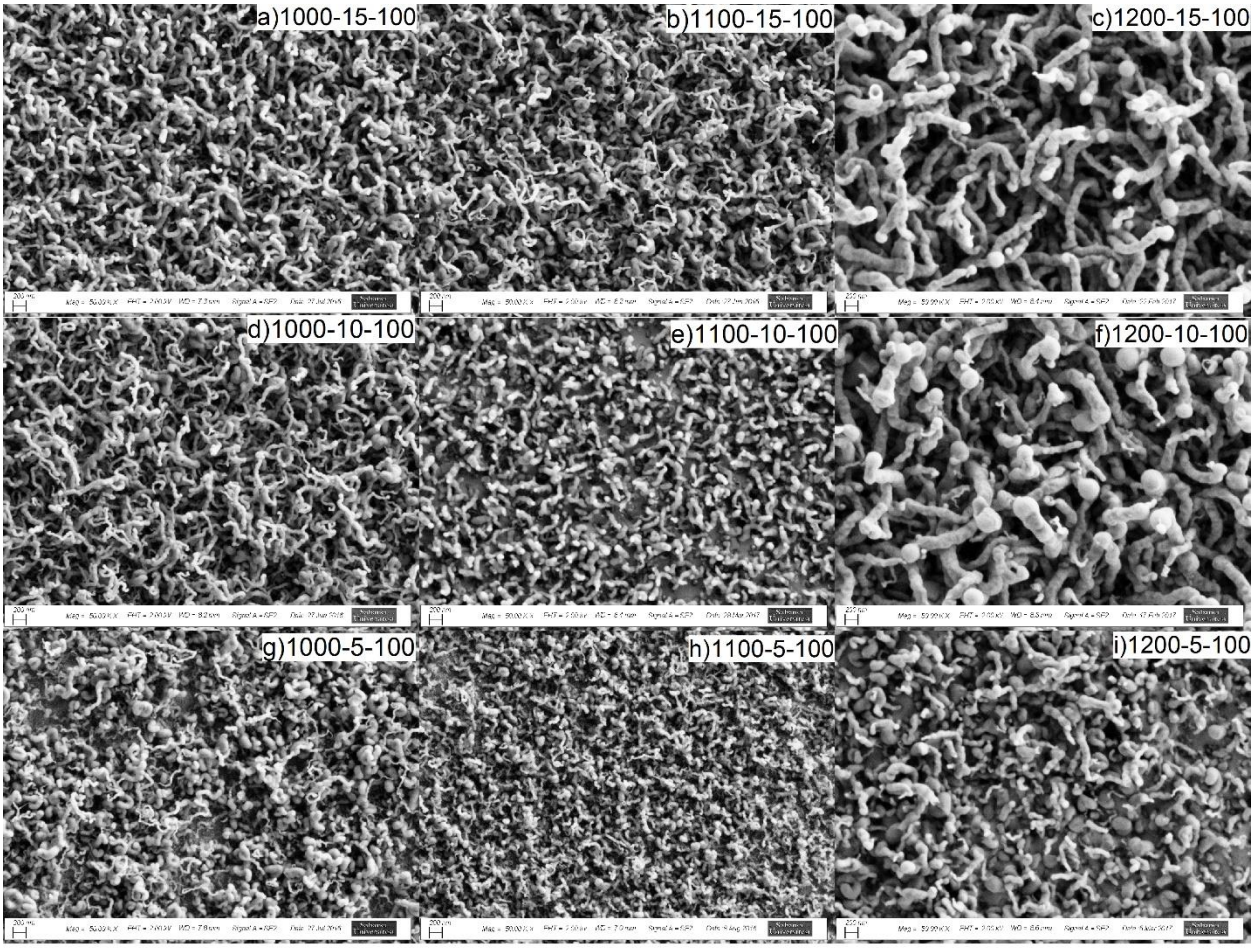

Figure 20: SEM images of BNNTs produced under 100 ml/min NH_3 flow rate (Right top: Experimental point)

Table 2:Diameter Measurements of Nanotubes

Reaction Temperature (˚C)	Heating Rate (˚C/min)	NH_3 Flow Rate (ml/min)	Diameter (nm)	Standard Deviation
1000	5	100	40.20	18.63
1000	5	150	43.39	18.58
1000	5	200	36.10	13.38
1000	10	100	47.61	11.78
1000	10	150	62.14	27.38
1000	10	200	45.62	19.23
1000	15	100	42.77	12.42
1000	15	150	73.60	26.99
1000	15	200	47.40	18.45
1100	5	100	37.64	12.34
1100	5	150	41.89	14.05
1100	5	200	27.23	6.81
1100	10	100	55.15	15.04
1100	10	150	59.65	28.63
1100	10	200	57.75	28.69
1100	15	100	38.47	11.02
1100	15	150	54.22	22.76
1100	15	200	46.23	18.99
1200	5	100	62.38	19.60
1200	5	150	44.46	17.62
1200	5	200	52.30	21.32
1200	10	100	109.92	56.81
1200	10	150	51.71	21.95

1200	10	200	62.38	19.60
1200	15	100	92,33	33.52
1200	15	150	54.35	22.78
1200	15	200	55.15	20.83

2.4.1.3 Raman Spectroscopy Results

Raman spectroscopy results for positions and intensities of BN and Si peaks are given in Table 3. Calculated BNNT film thickness results are given in Table 4.

Table 3:Peak Positions and Intensities of BN and Si

Reaction Temperature (˚C)	**Heating Rate (˚C/min)**	**NH_3 Flow Rate (ml/min)**	**BN Peak (cm^{-1})**	**Intensity**	**Si Wafer Peak (cm^{-1})**	**Intensity**
1000	5	100	1367	59428	523	89551
1000	5	150	1370	20010	520	70853
1000	5	200	1361	20668	522	109484
1000	10	100	1363	20240	521	89061
1000	10	150	1367	31968	520	45922
1000	10	200	1367	11648	522	89591
1000	15	100	1365	20211	517	92284
1000	15	150	1361	23588	520	48337
1000	15	200	1365	7119	519	79865
1100	5	100	1368	42467	519	44494
1100	5	150	1371	31974	520	45922
1100	5	200	1360	19538	519	39061
1100	10	100	1365	17258	519	56730
1100	10	150	1363	31422	520	20933

1100	10	200	1360	26042	519	17853
1100	15	100	1367	45129	519	69560
1100	15	150	1367	36650	520	30910
1100	15	200	1367	19529	520	31380
1200	5	100	1368	59751	516	50946
1200	5	150	1370	48844	518	33133
1200	5	200	1366	47943	515	26131
1200	10	100	1367	42237	515	23523
1200	10	150	1368	40152	517	25819
1200	10	200	1368	62566	518	36569
1200	15	100	1366	24960	516	14542
1200	15	150	1369	46092	518	29517
1200	15	200	1365	34992	518	19910

Table 4:BNNT Film Thickness Values

Reaction Temperature (˚C)	**Heating Rate (˚C/min)**	**NH_3 Flow Rate (ml/min)**	**Thickness (µm)**
1000	5	100	2.03
1000	5	150	1.78
1000	5	200	1.93
1000	10	100	1.98
1000	10	150	1.88
1000	10	200	1.72
1000	15	100	1.96
1000	15	150	1.95
1000	15	200	1.53

1100	5	100	2.04
1100	5	150	2.00
1100	5	200	2.03
1100	10	100	2.06
1100	10	150	2.07
1100	10	200	2.11
1100	15	100	2.10
1100	15	150	1.98
1100	15	200	2.06
1200	5	100	2.16
1200	5	150	2.14
1200	5	200	2.16
1200	10	100	2.19
1200	10	150	2.09
1200	10	200	2.15
1200	15	100	2.15
1200	15	150	2.10
1200	15	200	2.16

2.4.1.4 Statistical Analyzes

Polynomial regression models were developed using a full factorial design to analyze the effects of parameters (reaction temperature (X_1), heating rate (X_2) and reactive gas (NH_3) flow rate (X_3)) and their interactions on the diameter (Y_1), aspect ratio (Y_2) and wafer coverage ratio (Y_3) of the BNNTs. The response values are obtained from the experiments and shown in Table 5. The average diameter of the nanotubes changed between 36 to 110 nm, aspect ratio of the tubes ranged from 26 to 55 and the wafer coverage metric (ratio of BN peak to Si peak) varied from 0.13 to 1.83. Experimental errors were calculated from all 27 experiments.

Table 5:Full Factorial Design Matrix for BNNT Production

	Levels					
Run	X_1	X_2	X_3	Y_1: Diameter (nm)	Y_2: Aspect Ratio (μm/ μm)	Y_3: Wafer Coverage Ratio
1	-1	-1	-1	40.20	50.48	0.66
2	-1	-1	0	43.39	41.15	0.28
3	-1	-1	1	36.10	53.46	0.18
4	-1	0	-1	47.61	41.58	0.22
5	-1	0	0	62.14	30.40	0.69
6	-1	0	1	45.62	37.69	0.13
7	-1	1	-1	42.77	45.81	0.21
8	-1	1	0	73.60	26.49	0.48
9	-1	1	1	47.40	32.27	0.08
10	0	-1	-1	37.64	54.18	0.95
11	0	-1	0	41.89	47.73	0.69
12	0	-1	1	27.23	74.53	0.50
13	0	0	-1	55.15	37.34	0.30
14	0	0	0	59.65	34.70	1.50
15	0	0	1	57.75	36.53	1.45
16	0	1	-1	38.47	54.68	0.64
17	0	1	0	54.22	36.51	1.18
18	0	1	1	46.23	44.63	0.62
19	1	-1	-1	62.38	34.62	1.17
20	1	-1	0	44.46	48.12	1.47
21	1	-1	1	52.30	41.32	1.83
22	1	0	-1	109.92	20.01	1.79
23	1	0	0	51.71	40.58	1.55
24	1	0	1	62.38	34.54	1.71
25	1	1	-1	92.33	23.28	1.71
26	1	1	0	54.35	38.80	1.56
27	1	1	1	55.15	39.21	1.75

The P-value in statistical studies indicates the probability of errors stating that there is a significant evidence for obtained results explained by the model and its terms [50]. Smaller values of P-value mean that the relevant coefficient terms are significant, and not zero [51]. The fitting models for each response were developed in terms of coded parameters after excluding the insignificant terms (i.e. P>0.05) and are given below (Eq 4-6)

$$Y_1 = +54{,}39+8{,}12X_1+6{,}61X_2-5{,}35X_3-7{,}78X_1*X_3+10{,}41X_1^2-11{,}88X_2^2 \quad (4)$$

$$Y_2 = +40{,}82-2{,}16X_1-5{,}77X_2+1{,}79X_3-4{,}30X_1*X_3+8{,}99X_1^2+8{,}92X_2^2 \quad (5)$$

$$Y_3 = +0{,}94203+0{,}644X_1+0{,}0289X_2+0{,}0327X_3 \quad (6)$$

Another approach for statistical analysis is the desirability function. The desirability function (d) is used to obtain optimum solutions for multiple response systems. The general approach in this method is to find individual desirability function for each response at first and then to find maximum values of overall desirability function, D, by changing parameters. The values of desirability function vary between 0 to 1. If the desirability function value is 1, it means the response achieves its target and if its value is 0, it means that the response's value is not in an acceptable range [18].

2.4.1.5 Model Evaluation

The accuracy of models was evaluated by the coefficient of determination value, R^2. Figure 21 shows the predicted values against the experimental values of the diameter, aspect ratio and wafer coverage. Figures show the predicted values are not fully in agreement with experimental data. The R^2 values for the equations 3-5 were found as 61%, 59% and 77%, respectively.

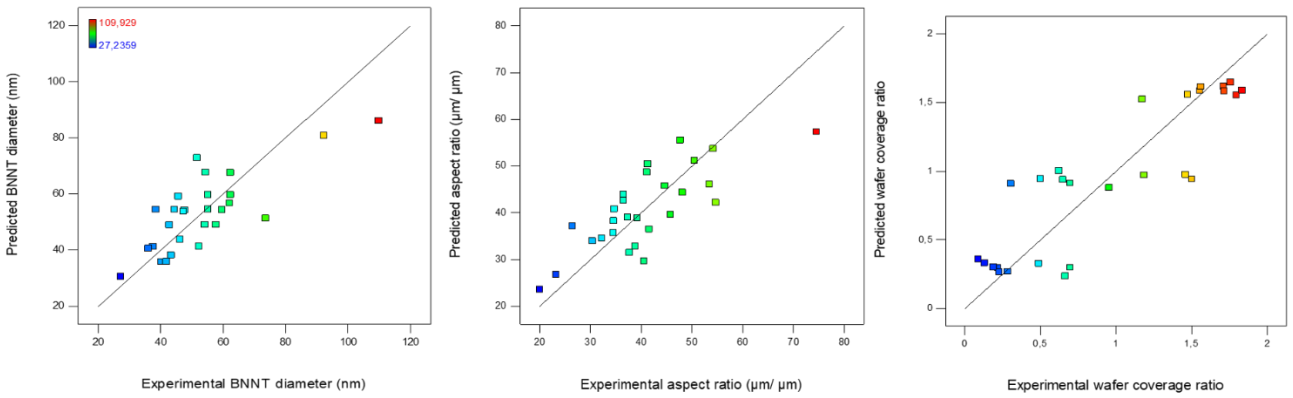

Figure 21:a)Predicted vs experimental diameter of BNNTs, b) Predicted vs experimental aspect ratio of BNNTs, c) Predicted vs experimental wafer coverage

Addition to predicted against experimental values analysis, the evidence of need for models to explain the data was examined by investigating the residuals. Figure 22 shows the normal plots of residuals and residual against predicted plots for diameter, aspect ratio and wafer coverage. The normal probability plots show how the residuals follow a normal distribution which is a basic assumption on the randomness of the experimental errors. If there is a straight line in plots, it means that residuals follow a normal distribution [20].Although there were some scattering in the data, they generally followed a straight line. Thus, the results indicate that data had a normal behavior for all responses.

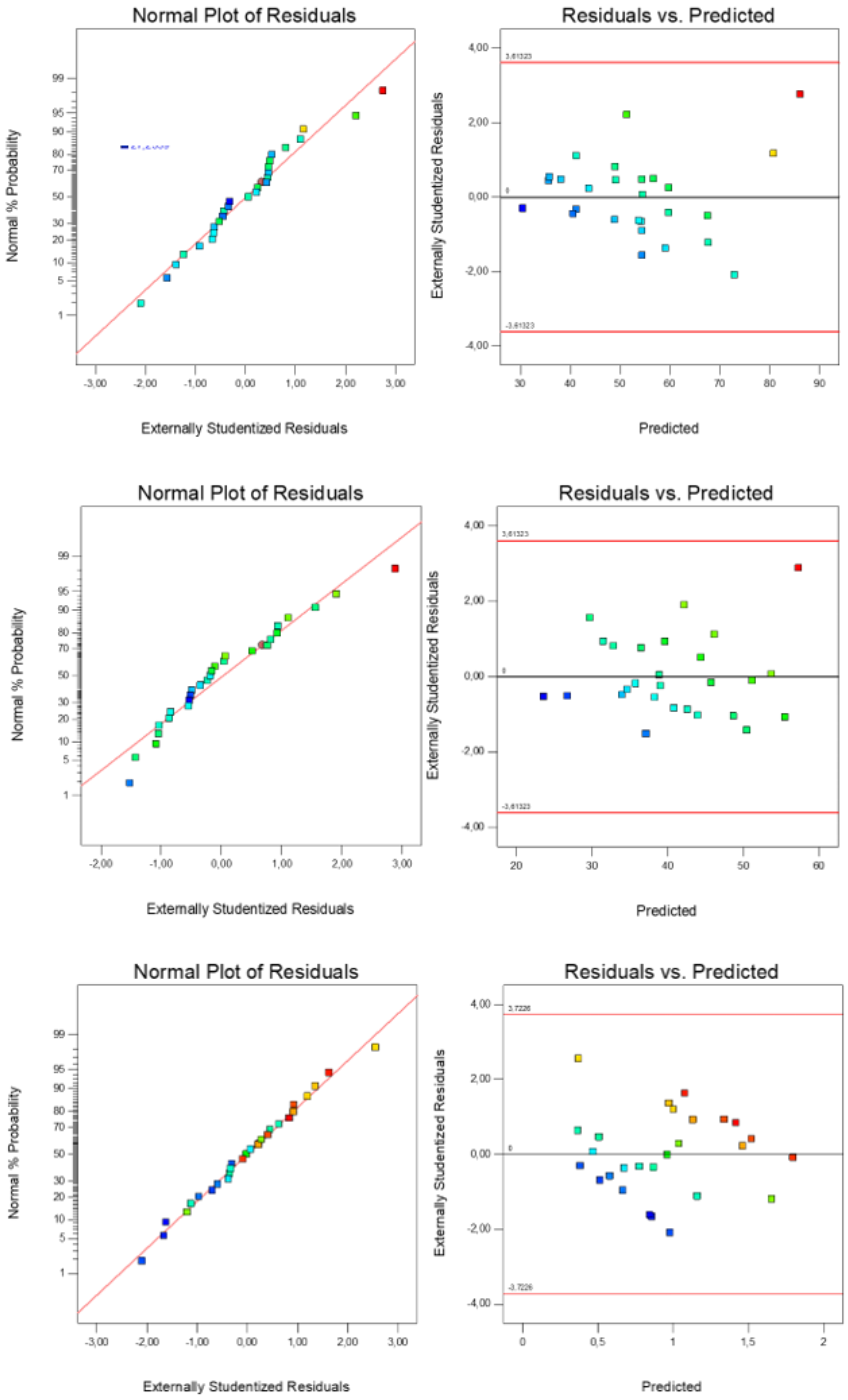

Figure 22:Normal plot of residuals and residuals versus predicted plots for a), b) Diameter, c), d) Aspect ratio and e), f) Wafer coverage

Finally, the significance of models was evaluated by analysis of variance (ANOVA). The ANOVA results for quadratic models of diameter and aspect ratio are listed in Tables 6 and 7, while linear model for wafer coverage is listed in Table 8. The model F values for diameter and aspect ratio were 5.32 and 5 which indicate that both models were significant with P-values of less than 1%. The probability values of the models show the possibility of obtaining F values just by randomness, but not an underlying model. Thus, having lower values are favorable for an existing model [18]. The probability values of models for diameter, aspect ratio and wafer coverage were 0.0020, 0.0028 and <0.0010, respectively. In cases for both diameter and the aspect ratio of nanotubes, reaction temperature (X_1), heating rate (X_2), reactive gas flow rate (X_3) and some of their interaction terms (X_1*X_3, X_1^2, X_2^2) were significant terms for models according to their P values. F value for wafer coverage was 25.78 which made the term significant as well. For this case, reaction temperature (X_1), heating rate (X_2) and reactive gas flow rate (X_3) were only significant terms, whereas their interaction terms were insignificant for the model given the available data.

Table 6:Analysis of ANOVA for Response Surface Quadratic Model for BNNT Diameter

Source	Sum of Squares	Degree of freedom	Mean Square	F Value	Prob>F	
Model	4709.89	6	784.98	5.32	0.0020	significant
X_1	1186.66	1	1186.66	8.04	0.0102	
X_2	785.80	1	785.80	5.32	0.0319	
X_3	515.31	1	515.31	3.49	0.0764	
X_1*X_3	726.03	1	726.03	4.92	0.0383	
X_1^2	650.00	1	650.00	4.40	0.0488	
X_2^2	846.09	1	846.09	5.73	0.0266	

Table 7:Analysis of ANOVA for Response Surface Quadratic Model for BNNT Aspect Ratio

Source	Sum of Squares	Degree of freedom	Mean Square	F Value	Prob>F	
Model	1925.59	6	320.93	5.00	0.0028	significant
X_1	83.85	1	83.85	1.31	0.2667	
X_2	599.85	1	599.85	9.34	0.0062	
X_3	57.60	1	57.60	0.90	0.3549	
X_1*X_3	221.97	1	221.97	3.46	0.0778	
X_1^2	485.10	1	485.10	7.55	0.0124	
X_2^2	477.22	1	477.22	7.43	0.0130	

Table 8:Analysis of ANOVA for Response Surface Linear Model for Wafer Coverage

Source	Sum of Squares	Degree of freedom	Mean Square	F Value	Prob>F	
Model	7.52	3	2.51	25.90	< 0.0001	significant
X_1	7.49	1	7.49	77.36	< 0.0001	
X_2	0.014	1	0.014	0.14	0.7083	
X_3	0.020	1	0.020	0.21	0.6537	

2.4.1.6 Effects of Parameters on Diameter of BNNTs

ANOVA results showed that reaction temperature and heating rate had significant effects on diameter of nanotubes while reactive gas flow rate was the least affecting factor. Reaction temperature and heating rate both affected the response individually and proportionally to square of the parameters while reaction temperature and reactive gas flow found interactively affecting the diameter of the nanotubes. Figure 23 shows the three-dimensional response surface plot which demonstrates the effects of reaction temperature and heating rate on the diameters of BNNTs when the reactive gas flow rate was fixed at +1 level. As can be seen from the Figure 23, minimum heating rate results in narrower diameters whereas mid-level reaction temperature gives the minimum diameter values.

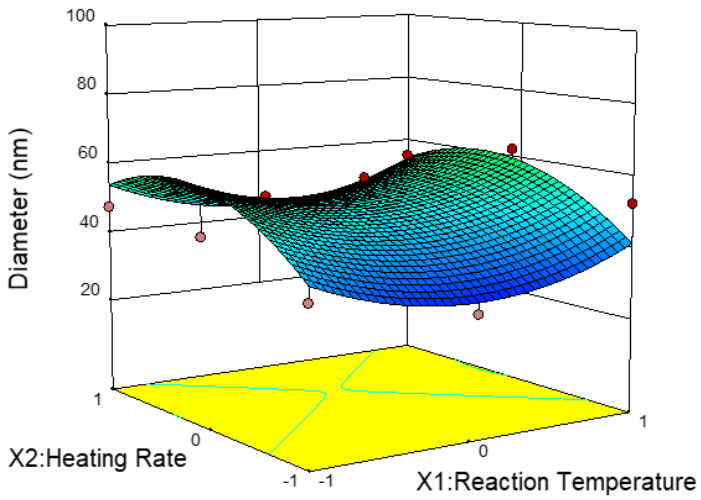

Figure 23:Three-dimensional response surface plot showing the effects of reaction temperature and heating rate on diameter of BNNTs (Reactive gas flow rate is fixed at +1 level.)

The desirability functions were calculated by the Design Expert Software and the possible solutions were found to determine the optimum reaction conditions for minimum diameter of nanotubes. The most desirable solution was found as reaction temperature of 1098˚C, heating rate of 5˚C/min and reactive flow rate of 200 ml/min with a desirability function value of 0.960. The diameter predicted under these conditions was 30.55 nm which was in a good agreement in our experimental diameter value of 27.23 nm for reaction temperature of 1100˚C, heating rate of 5˚C/min and reactive flow rate of 200 ml/min. Also, it was notable that most of the suggested solutions required minimum heating rate and maximum reactive gas flow rate.

2.4.1.7 Effects of Parameters on Aspect Ratio of BNNTs

ANOVA results showed that reaction temperature and heating rate had significant effects on aspect ratio of the nanotubes while reactive gas flow rate was the least effective similar to the case of diameter. Both of reaction temperature and heating rate affected the response individually and proportionally to the square of the parameters. Figure 24 shows the three-dimensional response surface plot which demonstrates the effects of reaction temperature and heating rate on the aspect ratio of BNNTs when the reactive gas flow rate was fixed at 0 level.

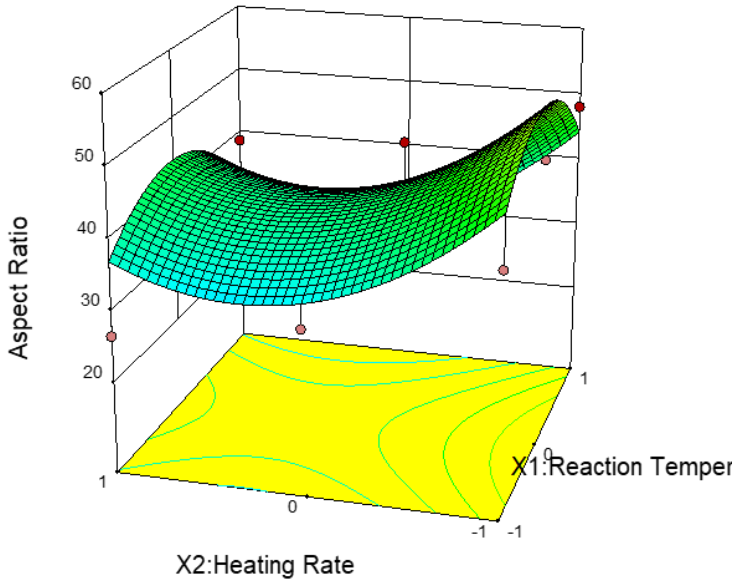

Figure 24:Three-dimensional response surface plot showing the effects of reaction temperature and heating rate on aspect ratio of BNNTs (Reactive gas flow rate is fixed at 0 level.)

The desirability functions were calculated by the Design Expert Software and the possible solutions were found to determine the optimum reaction conditions for maximum aspect ratio of the nanotubes. The most desirable solution was found as reaction temperature of 1110˚C, heating rate of 5˚C/min and reactive flow rate of 200 ml/min with a desirability function value of 0.686. The aspect ratio predicted under these conditions was 57.427. Also, it was notable that most of the suggested solutions required minimum heating rate and maximum reactive gas flow rate.

2.4.1.8 Effects of Parameters on Wafer Coverage of BNNTs

ANOVA results showed that all reaction temperature, heating rate and reactive gas flow rate had significant effects on the wafer coverage. The predicted model was a first order polynomial model, no interaction was noted. Figure 25 shows the three-dimensional response surface plot which demonstrates the effects of reaction temperature and heating rate on wafer coverage of BNNTs when the reactive gas flow rate was fixed at 0 level. Figure 26 demonstrates how the wafer coverage is related to the Raman shift intensities. When the wafer is more coated, the signal coming from the specimen is more significant which results in higher intensity. On the other hand, signal coming from the wafer increases when the coating is not sufficient.

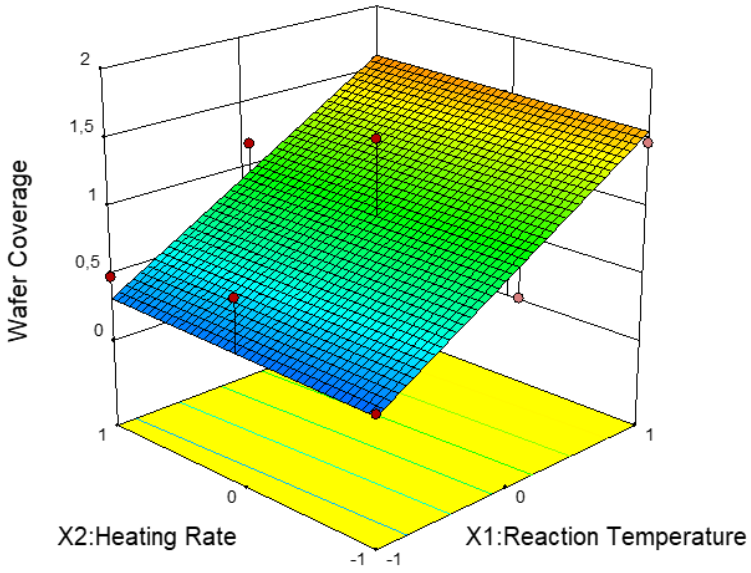

Figure 25:Three-dimensional response surface plot showing the effects of reaction temperature and heating rate on wafer coverage of BNNTs (Reactive gas flow rate is fixed at 0 level.)

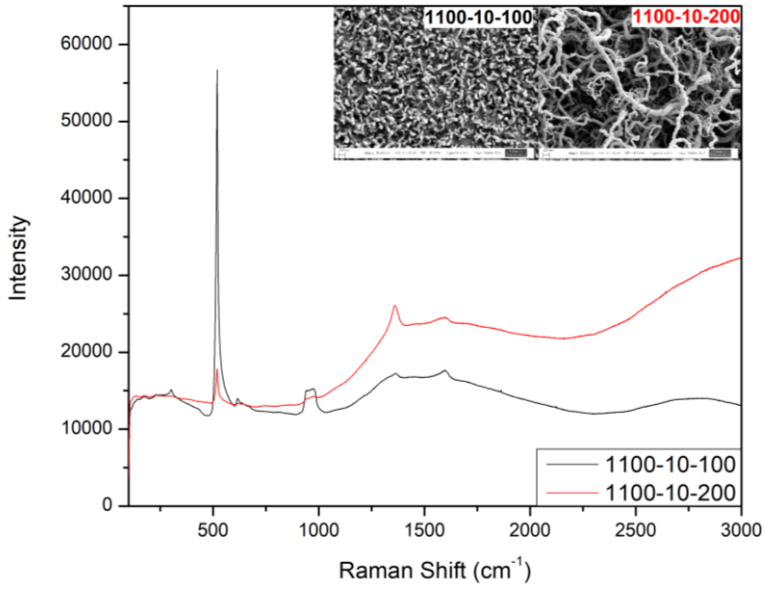

Figure 26: An example for relation of wafer coverage Raman shift intensities

The desirability functions were calculated by the Design Expert Software and the possible solutions were found to determine the optimum reaction conditions for maximum wafer coverage of the nanotubes. The most desirable solution with a desirability function value of 1, was reaction

temperature of 1200˚C, heating rate of 15˚C/min and reactive flow rate of 200 ml/min. The wafer coverage predicted under these conditions was found as 1.648. Also, it was notable that most of the suggested solutions required maximum reaction temperature, maximum heating rate and maximum reactive gas flow rate.

2.4.1.9 Optimization of Process Conditions by Multiple Response Surface Methodology

The results of the optimization studies for three different responses were different than each other due to their differences in the region of interest for each factor. Thus, a multiple response surface optimization study was required to obtain a compromised solution. Objectives for this study were chosen as aspect ratio and wafer coverage since diameter results were already included in aspect ratio values. The desirability function was used to find optimum solution for maximum aspect ratio and maximum wafer coverage.

The most desirable solution was reaction temperature of 1191˚C, heating rate of 5˚C/min and reactive flow rate of 200 ml/min with a desirability function value of 0.94. The aspect ratio of the nanotubes was predicted as 51.82 and the wafer coverage was predicted as 1.53 which were in a good agreement in our experimental aspect ratio and wafer coverage values of 41.32 and 1.83 for reaction temperature of 1200˚C, heating rate of 5˚C/min and reactive flow rate of 200 ml/min. Also, it was notable that most of the suggested solutions required very close values to maximum reaction temperature, while they require minimum heating rate and maximum reactive gas flow rate.

2.5 Conclusions

A full factorial experimental design was conducted to study the effects of reaction temperature, heating rate and reactive gas flow rate on diameter, aspect ratio and wafer coverage of BNNTs. Empirical models were developed to understand system's behavior. Experimental values and predicted results from the developed models showed a reasonable agreement for each response. A multiple response surface optimization study was performed to determine a compromised solution which satisfies each response as possible. The optimum conditions for maximum aspect ratio and maximum coverage was found as 1190˚C reaction temperature, 5˚C/min heating rate and 200 ml/min reactive gas flow rate.

3 Chapter 3: Effects of Boron Nitride Nanotubes (BNNTs) on Epoxy Resin Curing

3.1 Introduction

Thermoset polymers are widely used as matrix part of the composite materials [25, 26].Their main difference from thermoplastic polymers is that they experience chemical reactions through their use while thermoplastics only experience reversible physical changes such as melting [27]. Among them, epoxy resins have attracted the attention the most due to their superior properties such as high modulus, low shrinkage in cure, good adhesion, good chemical and corrosion resistance. Also, the properties of the uncured epoxy resin such as viscosity makes it easy to process and shape. Moreover, their reasonable cost and light weight make them promising materials [26-29]. Due to such interesting properties of epoxy resins, they have a wide range of application areas including high performance composites and electronics. [26, 30-32].

It is well known that the curing reaction of epoxy resin is an important factor for the properties of the final product. Linear epoxy monomers are linking to each other to form a three-dimensional crosslinked network during the curing process in which viscosity of the thermosets progressively increases causing a decrease in mobility of polymer chains until it becomes fully solidified. [27, 33]. Another effecting factor on the properties of the final product is the addition of filler materials. Typically, many thermosets are used in reinforced or filled form to tune their physical properties and characteristics and/or to reduce their costs [27, 34].

Since the discovery of nanotube structures in 1991 [35], the interest in nanotube/polymer nanocomposites has increased and created a new class of reinforced materials [31]. More specifically, improvements of the various properties of epoxy resins by adding nanotubes have been widely studied [31, 33, 36, 37]. The most of the initial studies was performed by using carbon nanotubes (CNTs) due to their impressive properties such as high aspect ratio, good thermal and electrical conductivity and superior mechanical properties [32, 36, 38]. Another promising alternative to prepare such nanotube/epoxy resin nanocomposites is boron nitride nanotubes (BNNTs). BNNTs are structural analogues of carbon nanotubes (CNTs) in which alternating B and N atoms replace C atoms with almost no interatomic space change [1, 2]. BNNTs were theoretically anticipated and first synthesized in 1995 [3]. Similar to CNTs, BNNTs exhibit superior thermal and mechanical properties [4, 5]. In addition, they have higher chemical stability

than CNTs [6]. One important difference between these nanotubes is related to their electronic structure. BNNTs are good insulators with a wide band gap (~5.5 eV) which is independent from chirality, diameter and number of walls whereas CNTs are conductive materials with a narrow band gap [1, 7, 8]. Addition to these, alternating B and N atoms in the structure with different affinities result in polarization of B-N bond which may offer an advantage for better compatibility. In other words, BNNTs are expected have superior binding interfaces due to their polarized structures [39].

As mentioned before, nanofillers are widely used as reinforcing and enhancing agents for polymer composites. Idea of mechanically strong, thermally enhanced, electrically insulator, transparent or whitish and lightweight composites recalls BNNTs as good nanofiller candidate. There are much fewer studies for the different thermal and mechanical properties of BNNT/epoxy nanocomposites [40, 41] compared to CNTs. Yet there is not a well-established study related to the effects of BNNTs on the curing mechanisms of epoxy resins which is very crucial for composite processing. As for guiding work, again one can find numerous studies for the curing mechanisms of different types of CNT/epoxy resin nanocomposites. Zhou et al.[33] suggested that addition of multi walled CNTs to epoxy imidazole system created an acceleration effect on the overall curing. Puglia et al.[36] demonstrated that single wall CNTs incorporated into diglycidyl ether of bisphenol A-based (DGEBA) epoxy resin acted as a strong catalyst for curing system. Xie at al. [32] studied the effects of addition of multi wall CNTs into tetraglycidyl-4,4’-diaminodiphenylmethane /4,4-diaminodiphenylsulfone (TGDDM/DDS) system which showed that CNTs had an acceleration effect on the cure reaction.

It is known that, highly cohesive Van der Waals forces and hydrophobic properties of BNNTs make it difficult to form homogenous dispersion in aqueous medium [52]. Also, literature review showed that better dispersion can be achieved by surface functionalization of nanotubes which enhances the reactivity of nanofillers. Therefore, better interfacial bond can be formed in polymer matrices which may prevent agglomerations and increase their compatibility [31, 37]. Thus, there are few studies focusing on surface functionalization of BN based nanofillers. For instance, Lee et al. [37] studied the effects of surface modifications on hexagonal boron nitride nanoflakes in polymer matrix by noncovalent modifications. They concluded that functionalization increased the surface area between nanoflakes and polymer and therefore improved the physical properties. Yan

et al. [52] worked on noncovalent functionalization of BNNTs to increase compatibility between nanotubes and epoxy resin to improve physical properties. Thus, one can suggest that surface functionalization should be applied on BNNTs to improve dispersion inside polymer matrix. But in this study unfunctionalized (as-synthesized) form of BNNTs were preferred since this work is considered as an initial cure mechanism study.

The main focus of this chapter is to comprehend the effects of BNNTs on cure mechanism of epoxy resin systems. Therefore, different weight fractions of BNNTs were added into epoxy resin/hardener systems. Cure behavior of the prepared nanocomposites was observed by mainly dynamic and isothermal scanning measurements.

3.2 Cure Mechanism of Epoxy Resins

Uncured thermoset polymers usually consist of monomers and hardener molecules. Cure reaction or curing is an exothermic process which starts when linear monomers begin to form longer chains and branches. Through the cure reaction molecular mass continues to increase in an accelerated manner and eventually monomers form a linked network of infinite molecular mass (Figure 27). As the curing proceeds, an irreversible transformation occurs due to creation of new chemical bonds between monomers and this transformation from liquid to elastic gel state is called as gel point or gelation. Basically, gelation is the early stages of forming a crosslinked network and it is the most distinguishable property of thermoset materials. As the cure reaction continues, thermosets lose their ability to flow and when they exceed the gel point they are no longer further interfered. Nevertheless, the cure reaction remains unaffected by the gelation process. In other words, curing rate stays constant when the gelation occurs. Finally, fully cured and rigid structures are formed when the reaction proceeds beyond gel point [27, 53]

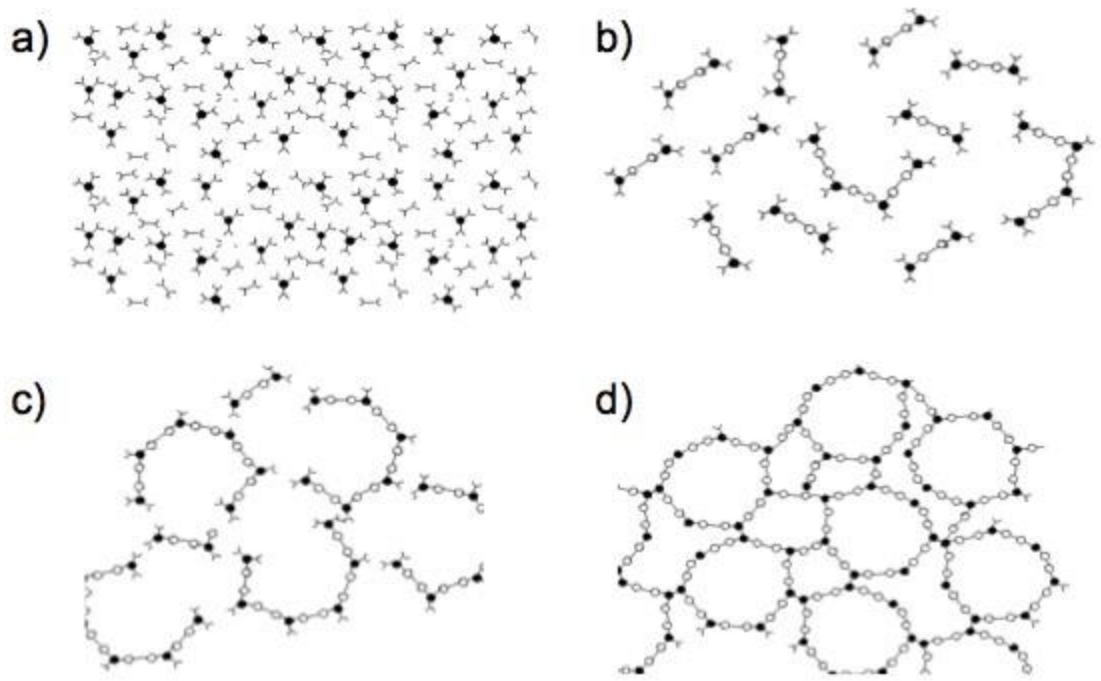

Figure 27:Illustration of thermoset curing a) Monomers b) Linear growth and branching c)Formation of crosslinked network (gelled but incomplete) d)Fully cured thermoset [27]

Epoxy resin is one of the widely used thermoset polymers which has at least two oxirane ring (C_2H_4O) or epoxy groups in their structures which are very reactive due to ring strain. Epoxide groups react with themselves and other groups to initiate curing reactions by forming crosslinked networks. As illustrated in Figure 28, nucleophilic attack on terminal carbon (C-O) causes bond to break which results in oxirane ring opening [31, 54]. Primary amine groups in hardener react with epoxy and form secondary amine groups which also react with remaining epoxy resin (Figure 29). Simultaneously, hydroxyl groups which are generated by the reaction between secondary amine hydrogen and epoxy results in formation of ether links by process called as etherification (Figure 30). In case of excess amount of epoxy ring or low activity of amine groups, etherification may compete with curing reaction. In order to avoid such cases cure temperature and stoichiometric ratio of epoxy/amine system should be chosen carefully [27, 31]. Moreover, overall cure reaction can be accelerated by the formation of secondary alcohols and hydroxyl groups which may serve as additional reactive sites.

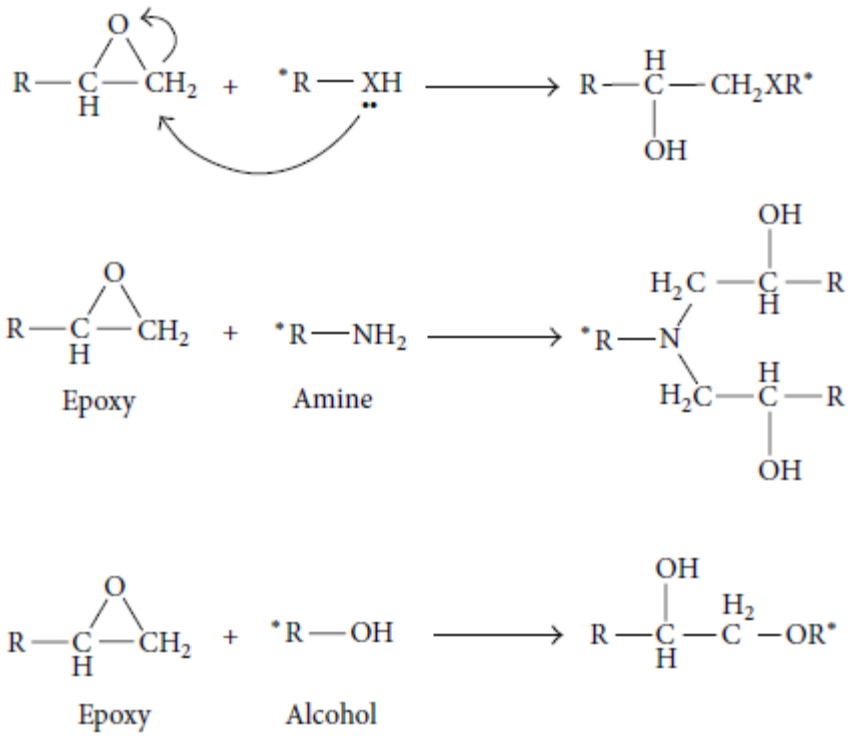

Figure 28:Oxirane opening mechanism via nucleophilic addition in epoxy systems [31]

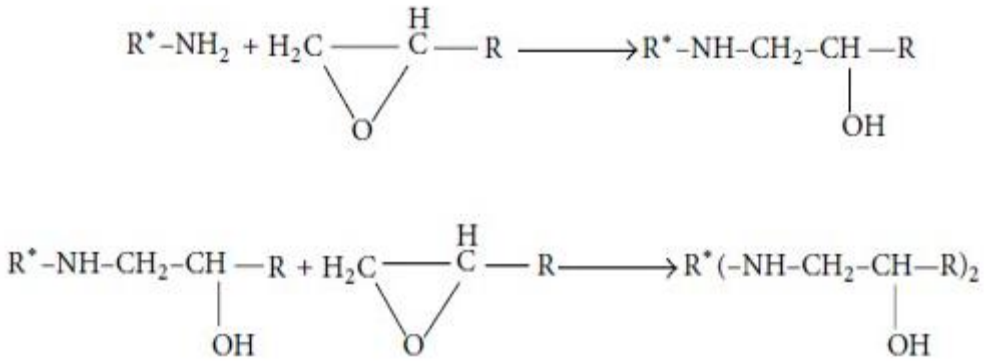

Figure 29:Curing mechanism of epoxy resins with amine based hardeners [31]

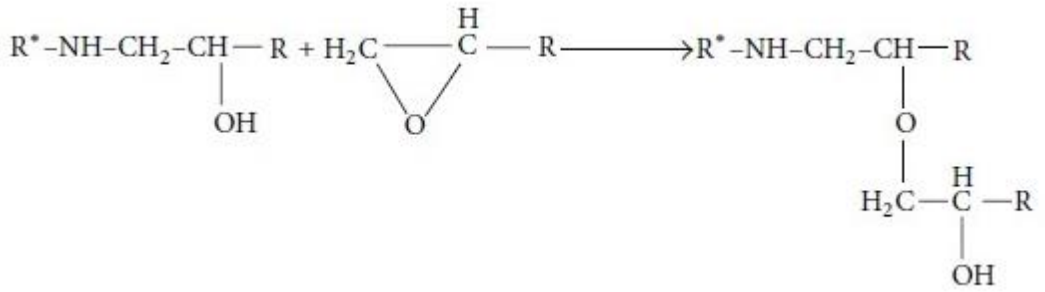

Figure 30: Mechanism of etherification reaction [31]

3.3 Cure Kinetics

Cure kinetics study is to reveal mathematical relationship between time, temperature and conversion. There are various methods used for analyzing cure kinetics of systems. Kissinger and Ozawa-Flynn-Wall methods were chosen for this cure kinetics study. Kissinger method assumes that activation energy remains constant through the cure reaction which is assumed to a be a first order reaction. It utilizes heating rate and peak temperature for kinetic model analysis as the following (Eq 7)

$$\ln\left(\frac{\beta}{T_p^2}\right) = \ln\left(\frac{AR}{E_a}\right) - \frac{E_a}{RT_p} \tag{7}$$

where β is heating rate, T_p is peak temperature of exotherm reaction, A is the pre-exponential factor, R is the universal gas constant and E_a is the activation energy. Values of E_a and A can be found by plotting $\ln(\beta/T_p^2)$ against $1/T_p$. The slope of the plotted graph gives E_a whereas the intercept gives A values [27, 29].

On the other hand, Ozawa-Flynn-Wall (OFW) method assumes that the activation energy of curing reaction changes as the reaction proceeds and it presumes the required amount of activation energy to decreases. Degree of cure (α) changes between 0 to 1 which correspond to uncured and fully cured systems. Similar to Kissinger method, OFW method uses heating rate and peak temperature of exotherm for kinetic model analysis as the following (Eq 8)

$$\log(\beta) = \frac{-0{,}457E_a}{RT} + A' \qquad A' = \log\left(\frac{AE_a}{g(\alpha)R}\right) - 2{,}315 \tag{8}$$

where β is heating rate, T is temperature, A is pre-exponential factor, $g(\alpha)$ is conversion dependent function, R is universal gas constant and E_a is activation energy. Values of E_a and A for each degree of cure can be found by plotting logβ against 1/T. The slope of the plotted graph gives E_a whereas the intercept gives A' values [27].

Area under the exothermic crosslinking curve gives the enthalpy value of the reaction (ΔH). As the reaction proceeds and system becomes partially cured, the required amount of enthalpy to complete cure reaction (residual enthalpy (ΔH_r)) is expected to decrease. The partial cure degree can be calculated by the area under the exothermic curve after isothermal process [27]. The following equation is used for the degree of cure calculations for isothermal cure analyzes (Eq 9)

$$\alpha = \frac{\Delta H - \Delta H_r}{\Delta H} \tag{9}$$

where α is degree of cure for partially cured systems in isothermal temperatures, ΔH is enthalpy of reaction obtained from dynamic measurements and ΔH_r is required amount of enthalpy to complete cure reaction after isothermal process [27].

Cure behavior of thermoset polymer systems are usually defined by the n^{th} order or autocatalytic models. The n^{th} order reaction model assumes that the rate of reaction only depends on unreacted reactants. This model successfully predicts the initial stages of curing, since it assumes that maximum reaction rate occurs at t=0. But it fails when system reaches the maximum reaction rates at the intermediate degree of cures [27]. Equation 10 below describes n^{th} order kinetic model;

$$\frac{d\alpha}{dt} = k(T)f(\alpha) = Aexp\left(-\frac{E_a}{RT}\right)(1-\alpha)^n \tag{10}$$

where $k(T)$ is temperature dependent rate constant, $f(\alpha)$ is reaction model, A is pre-exponential constant, E_a is activation energy, R is universal gas constant, α is degree of cure and n is reaction order.

The autocatalytic model assumes that at least one of the reaction products contributes to the overall reaction. This type of kinetic models usually characterized by maximum conversion degree of 20% to 60% at maximum rate [28]. Equation 11 describes the autocatalytic model;

$$\frac{d\alpha}{dt} = k(T)f(\alpha) = Aexp\left(-\frac{E_a}{RT}\right)(1-\alpha)^n(\alpha)^m \quad (11)$$

where *k(T)* is temperature dependent rate constant, *f(α)* is reaction model, *A* is pre-exponential constant, E_a is activation energy, *R* is the universal gas constant, *T* is temperature, *α* is degree of cure and *m* and *n* are reaction orders.

3.4 Experimental Procedure and Characterization

3.4.1.1 Materials

The liquid epoxy resin used in this study was a diglycidyl ether of bisphenol A (DGEBA) and the hardener was 4-4' methylenebis (cyclohexylamine) and isophrone diamine. Both epoxyr esin and hardener compounds were purchased from Huntsman (RenLam LY113 (epoxy)/Ren HY 98(hardener)). The chemical structures are presented in Figures 30 and 31.

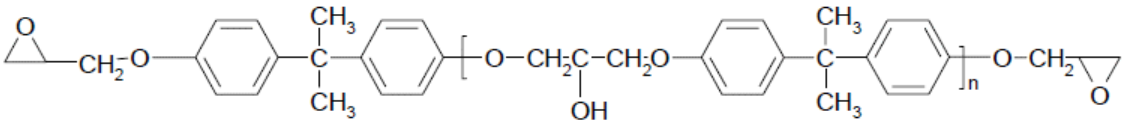

Figure 31:Chemical structure of DGEBA epoxy resin [29]

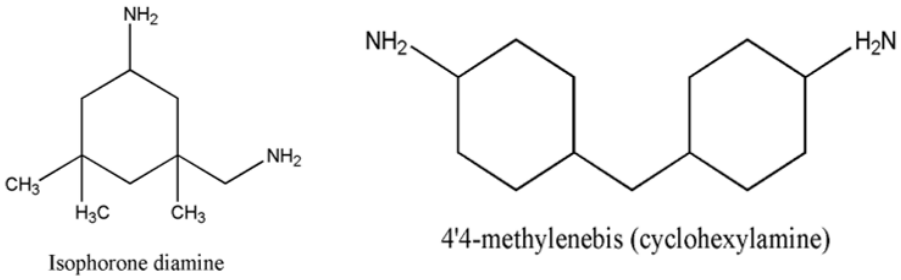

Figure 32:Chemical structures of amine-based hardener

Multiwalled boron nitride nanotubes (BNNTs) which were synthesized under obtained optimum synthesis conditions obtained from Chapter 2 were used for cure kinetics study. Thus, all the

BNNTs used for BNNT/epoxy nanocomposites were synthesized at 1200˚C with heating rate of 5˚C/min under the 200 ml/min NH_3 flow rate.

3.4.1.2 Sample Preparation

As a first step of sample preparation, produced BNNTs were collected from the surface of Si wafer. Literature review showed that there are two commonly used techniques: dissolving nanotubes in proper solvent and mechanical scratching. Latter one was chosen for this study since the first one may result in losing product. BNNTs were scratched from the surface of Si wafer by using a spatula. Figure 33 shows collected BNNTs in white color.

Figure 33: Collected BNNTs from the top of Si wafer by mechanical scratching

Dispersion of the collected BNNTs inside the epoxy matrix was the second step of the sample preparation. There are different approaches for addition of nanofillers [55, 56]. One of these approaches which was employed in this study is adding nanofillers to hardener first and adding epoxy afterwards. Collected BNNTs were added to hardener and sonicated for 1 hour to homogenize length of nanotubes. After the sonication BNNT/hardener solution was subjected to magnetic stirring for 15 hours to achieve homogenous dispersion of nanotubes inside the matrix. Then, required amount of epoxy was added to BNNT rich hardener by following 100:33 epoxy to hardener weight ratio. Samples containing 10.5 ± 0.5 mg nanocomposites were prepared for dynamic and isothermal DSC measurements. Figure 34 shows the illustration of BNNT/epoxy

nanocomposite and DSC sample preparation process. Storage of the prepared samples is very crucial for two-part epoxy resin/hardener systems, especially to prevent any unwanted reactions prior to actual measurements. A typical achievable criterion is allowing up to 1% reaction before the measurements. One suggested technique for moderately reactive systems in room temperature is to mix solution in room temperature and freeze until the measurement [27, 32, 33]. Thus, prepared samples were stored at freezer until the measurements. In addition to the DSC samples, samples for mass analyzes and dispersion analyzes were prepared from the same batch.

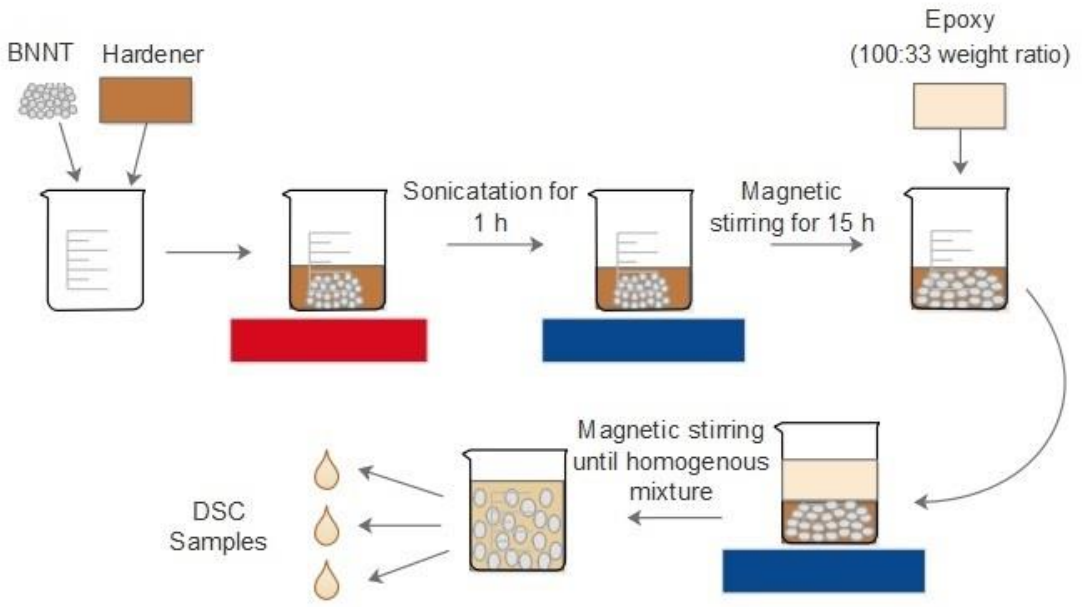

Figure 34:Illustration of BNNT/Epoxy resin nanocomposite preparation for DSC measurements

Five different weight fractions of BNNT/epoxy resin nanocomposites addition to neat epoxy were prepared by following the procedure above which were 0.25, 0.5,0.75,1 and 2wt% BNNT/epoxy resin nanocomposites.

3.4.1.3 Characterization Methods

3.4.1.4 Spectroscopic Characterizations

Fourier-transform infrared spectroscopy (FTIR) were performed to analyze cure reaction of epoxy resin/hardener system with Thermo Scientific Nicolet iS10 FTIR Spectrometer in mid-infrared region (between 600 and 4000 cm^{-1}) in Attenuated Total Reflection (ATR) mode.

3.4.1.5 Thermogravimetric Analyzes Measurements

Thermogravimetric analyzes of chosen samples were performed by using Shimadzu DTG-60H Simultaneous DTA-TG Apparatus to control mass content of prepared BNNT/epoxy nanocomposites. Analyzes were conducted between 30°C to 800°C with heating rate of 10°C/min under 100 ml/min nitrogen flow.

3.4.1.6 Microscopic Characterizations

SEM images of the BNNT/epoxy resin nanocomposites were taken with LEO Supra VP35 Field Emission Scanning Electron Microscope. Nikon Eclipse ME 600 Optical Microscope was used for distribution analysis of nanocomposites. Images were taken at 100x and 50x magnifications in dark field mode and cross polarizer was used.

3.4.1.7 Differential Scanning Calorimetry Measurements

Thermal properties of BNNT/epoxy resin nanocomposite specimens were probed by using TA Instruments Q2000 Differential Scanning Calorimeter (DSC). For dynamic DSC measurements, the temperature was ramped from 0°C to 250°C at five different heating rates (β), which were 2, 5, 10, 15 and 20°C/min in the first cycle. After cooling down to 0°C, a second heating cycle was performed up to 250°C with constant heating rate of 5°C/min to remove any prior thermal history. The first cycles of dynamic temperature scans were used to measure reaction enthalpies (ΔH) and reaction peak temperatures (T_p). The second cycle was used for determining T_g values. Isothermal DSC measurements were performed for 3 different isothermal waiting temperatures: 60°C, 85°C and 115°C which were chosen based on the onset and peak points of dynamic scan of uncured neat epoxy resin (0 wt% BNNT) with heating rate of 10°C/min. Samples were partially cured by waiting 5, 15, 30, 60, 90 and 120 minutes at isothermal temperatures. After the partial curing, samples

were cooled down to -30°C and heated up to 250°C by heating rate of 10°C/min. The second cycles of isothermal measurements were used to determine residual enthalpy and T_g values. All of the DSC measurements were performed under constant environment of nitrogen with flow rate of 50 ml/min. Analyzes of DSC measurement were performed by using TA Instruments Universal Analysis 2000 software.

3.5 Results and Discussion

3.5.1.1 Spectroscopic Analyzes

FTIR measurements were performed to follow the cure reaction of the epoxy resin/hardener system. Figure 35 a shows the FTIR spectra of amine-based hardener and epoxy resin separately. Figure 35 b shows only epoxy resin after curing. The observed two-shoulder peak around 3300 cm^{-1} in spectrum of hardener results from vibration movement of N-H bond stretching. Spectrum in Figure 35 b exhibits many characteristic peaks of epoxy resin: One around 1610 cm^{-1} corresponds to stretching of C=C of aromatic ring, one around 2900 cm^{-1} may correspond to stretching C-H of CH_2 and CH aromatic and one around 910 cm^{-1} corresponds to stretching C-O of oxirane ring in the structure [57]. When the spectrum of fully cured epoxy resin is examined, the peak around 3400 cm^{-1} hints the -OH formation due to oxirane ring opening which indicates curing reaction was successful.

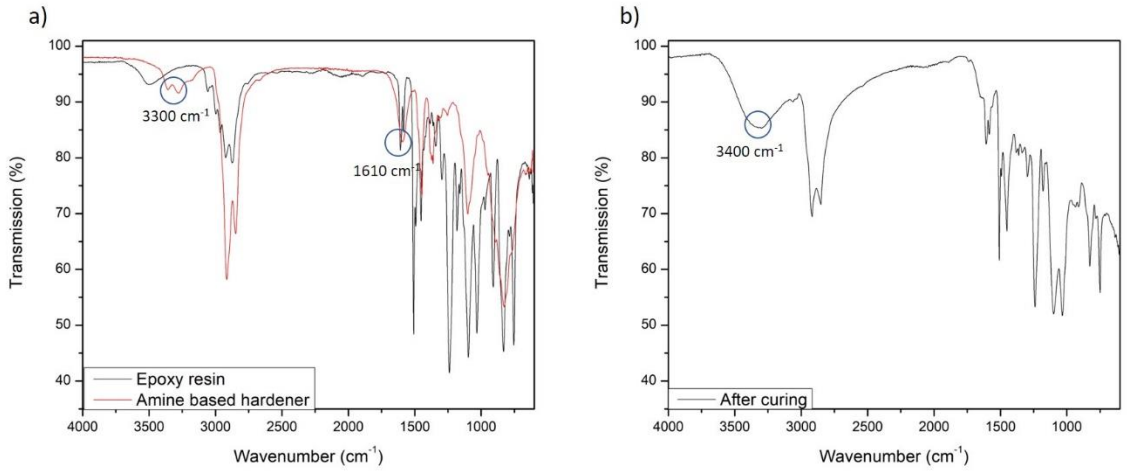

Figure 35:FTIR spectra of a) Epoxy resin and hardener b) Fully cured epoxy resin

3.5.1.2 Thermogravimetric Analyzes

It is known that BNNTs are thermally stable up to 1100˚C whereas the high performance epoxy resin starts to degrade approximately around 450˚C [58, 59]. Thus, ashes of epoxy resin and BNNTs are expected to remain after heating up to 800˚C. Consecutive measurements of neat and BNNT rich nanocomposites were performed for each weight ratio to get rid of the environmental conditions and to be able to assess the BNNT content. The mass analyzes showed reasonable outcomes for aimed BNNT weight fractions of 2%, 1% and 0.75% (Figure 36). But when it is lower than 0.75 wt%, results were inconclusive due to sensitivity of the instrument.

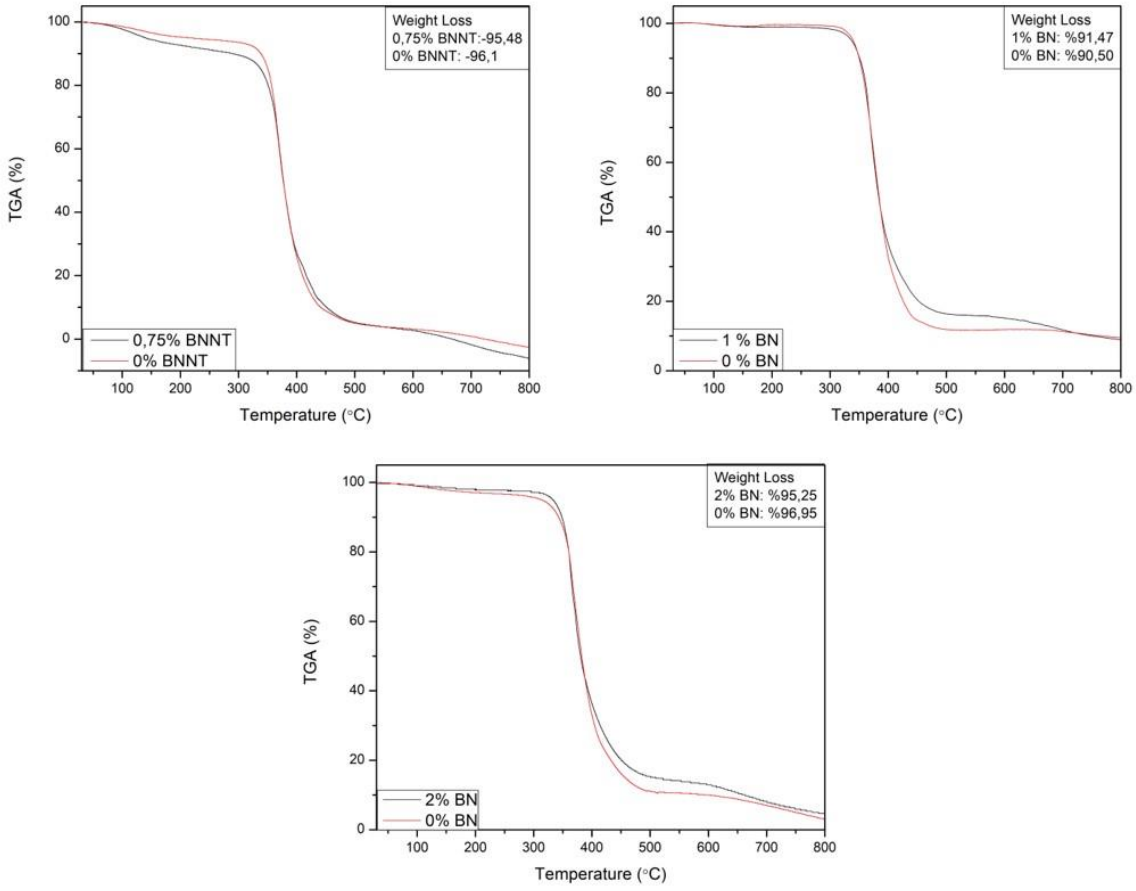

Figure 36:Obtained TGA curves of nanocomposites for different BNNT contents

3.5.1.3 Microscopic Analyzes

3.5.1.3.1 Optical Microscopy

It is known that epoxy resin polymers have an amorphous structure due to their crosslinked network which prevents formation of crystalline structures. On the other hand, BNNTs are crystalline [27, 60]. Epoxy resin exhibits an isotropic behavior in optical microscopy. In other words, since the chemical bonds formed in crosslinking are same at all directions, velocity of light does not change through the interaction. Thus, the dispersion of crystalline BNNT inside amorphous epoxy resin can be observed by optical microscopy. Figure 37 a and b show the optical microscopy images of 0.25 wt% BNNT and 0.75 wt% BNNT, respectively. Dark backgrounds in the images represent the epoxy resin while the inorganic nanotubes are observed as shiny particles. It was clear that BNNTs were dispersed homogenously in the epoxy matrix in 0.25 wt% BNNT/epoxy nanocomposite. Similarly, 0.75 wt% BNNT/epoxy nanocomposite had a good dispersion of nanotubes with local agglomeration regions of nanotubes.

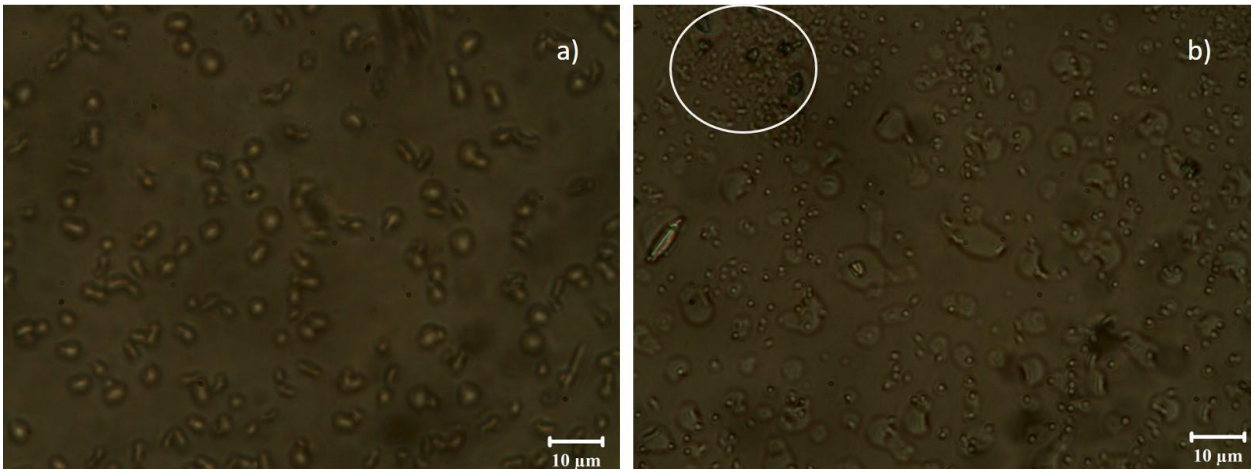

Figure 37:Optical microscopy images taken in dark field for dispersion of BNNTs inside epoxy resins a)0.25 wt% BNNT in 100x b)0.75 wt% BNNT in 50x

3.5.1.3.2 Scanning Electron Microscopy (SEM)

In addition to optical microscopy, scanning electron microscopy (SEM) was used to analyze dispersion of BNNTs inside epoxy matrix for 1 wt% and 2 wt% BNNT content nanocomposites. Mechanical test specimens after the fracture were used for this purpose. In accordance with the optical microscopy images which showed that 0.75% BNNT content nanocomposites had a good

dispersion with local agglomerations, 1 wt% had more frequent agglomeration regions of BNNTs (Figure 38 a b c). Also, 2 wt% BNNT content nanocomposites had almost no dispersion of nanotubes and they formed bulk agglomeration regions as seen in Figure 38 d. Thus, it can be concluded that 1 wt% BNNT content is the limit for good dispersion of nanotubes in epoxy resin matrix for this study.

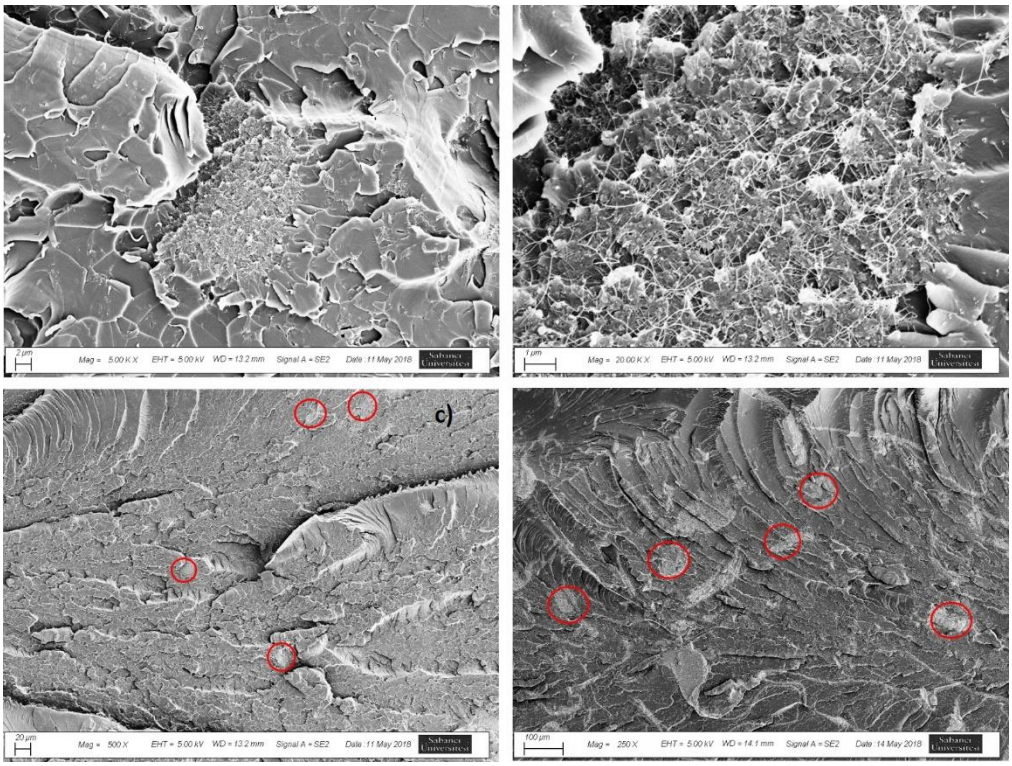

Figure 38:SEM images of specimens a-b-c) Tensile testing specimen of 1 wt% BNNT at 5K, 20K and 500X d)3PB specimen of 2 wt% BNNT at 250X

Agglomeration of nanotubes can stem from strongly cohesive Van der Waals forces between nanotubes[52]. Also, curly and entangled structures of BNNTs can contribute to cohesion and cause agglomerations. An improved dispersion can be achieved by surface functionalization which enhances the reactivity of nanofillers as seen in literature [37, 52]. Therefore, better interfacial bond can be formed in polymer matrices which may prevent agglomerations and increase compatibility of nanotubes [31, 37]. Thus, one can suggest that surface functionalization should be applied on BNNTs to improve dispersion inside polymer matrix.

3.5.1.4 Differential Scanning Calorimetry (DSC) Analyzes

3.5.1.4.1 Dynamic DSC Analyzes

The results of dynamic DSC measurements of different BNNT content/epoxy resin nanocomposites which were performed with different heating rates of 2, 5, 10, 15 and 20˚C/min are demonstrated in Figure 39.

A single broad exothermic peak was observed for each measurement which typically indicates that the system is governed by main curing reaction, not by side reactions. Thus, overall heat generated during the processes can be related to the curing [61]. Peak temperatures of exotherm were shifted to higher temperatures as the heating rate was increased. The reason of such behavior is that when the heating rate is slower, system has more tendency to become like-isothermal and to undergo chemical reactions accordingly. Thus, they can complete the curing at lower temperatures. But when the heating rate is higher, systems do not have enough time for reactions which leads to completion of curing reactions at higher temperatures to compensate time lack [61]. The obtained values of exothermic peak temperatures (T_p), glass transition temperatures (T_g) and enthalpy by dynamic measurements are listed in Table 9. When the results are examined, exothermic peak temperature values slightly decreased with the increasing BNNT content up to 0.75 wt %. Although 1 wt % and 2 wt % BNNT content nanocomposites reached the peak temperatures higher than 0.75 wt %, they were also at lower temperatures compared neat epoxy. Observed decrease is at all attributed to the dispersion quality of BNNTs inside epoxy resin. It can be noted that, BNNT filled epoxy resins reached faster to exotherm peak which is an indication for fast curing systems.

The glass transition temperature of a polymer defined as the critical temperature which melt or rubbery states changes into glassy state. The glass transition occurs in amorphous or amorphous fractions of semi crystalline polymers and T_g values depend on the mobility of polymer chains. The amorphous polymers are in glassy state and rigid form below their T_g values whereas they are in melt state above T_g values [27]. Thus, glass transition is very crucial for practical usage of polymers since it may also define limits for processing and usage temperatures. Results showed that T_g values exhibited a slight increase up to 0.75 wt % at which a sudden decrease in T_g was observed. Afterwards, T_g values continued to increase with increasing BNNT content. Increase in T_g with the addition of nanotubes can be attributed to constrained mobility of epoxy monomers.

Addition to physical hindrance of nanotubes, their accelerating effects at the initial stage of curing results in higher crosslinking density in epoxy resin matrix which leads to increase in T_g as well [31, 33]. On the other hand, sudden decrease in T_g at 0.75 wt % BNNT content can be attributed to homogenous dispersion of BNNTs inside epoxy matrix which creates extra free volume to allow big segmental motion of epoxy resin [33].

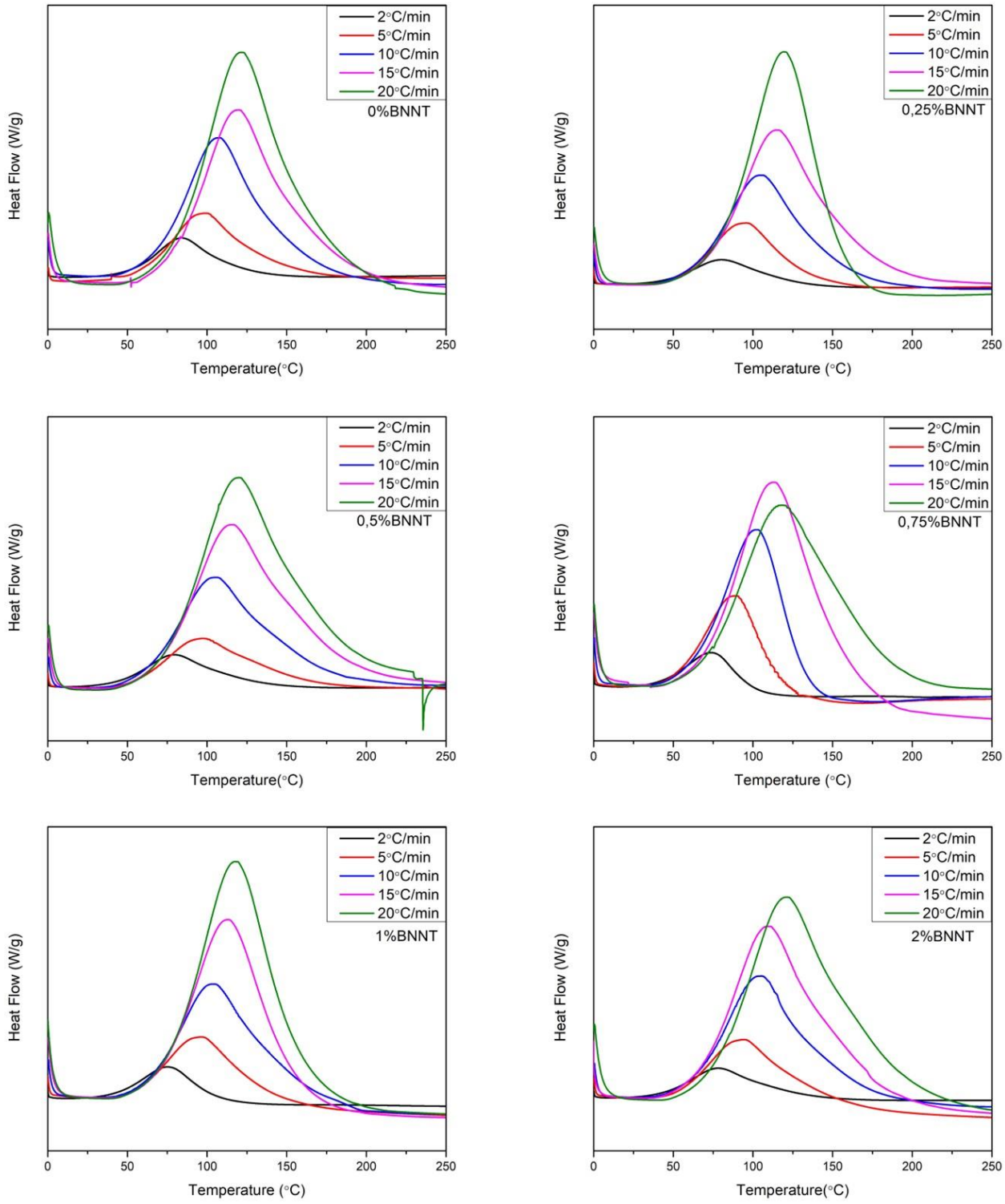

Figure 39: Dynamic DSC curves with different heating rates of the different BNNT content nanocomposites

Table 9: T_p, T_g and Enthalpy Values for Nanocomposites with Different BNNT Contents

BNNT Content	Heating Rate (˚C/min)	T_p (˚C)	T_g (˚C)
0 wt%	2	84.04	92.7
	5	98.67	98.71
	10	107.88	106.56
	15	120.44	110.07
	20	122.84	-
0.25 wt%	2	80.48	93.73
	5	96.10	96.71
	10	106.27	106.78
	15	116.20	111.78
	20	124.17	114.51
0.50 wt%	2	79.17	98.31
	5	98.03	110.74
	10	106.26	119.34
	15	116.64	119.95
	20	120.99	115.03
0.75 wt%	2	73.90	56.81
	5	89.31	55.51
	10	103.23	57.70
	15	113.85	96.10
	20	118.93	94.82
1 wt%	2	75.55	64.64
	5	97.24	96.32
	10	105.51	112.62

	15	114.11	72.30
	20	119.33	64.71
2 wt%	2	78.37	104.34
	5	94.92	113.62
	10	105.75	117.4
	15	114.25	119.97
	20	122.45	122.67

3.5.1.4.2 Kissinger Analyzes

As observed by the dynamic scans, T_p shifted to the higher temperatures with increasing heating rates. Main assumption in Kissinger method is that maximum heating rate is achieved at peak temperature of exotherm [28]. Thus, peak temperatures were used to calculate E_a and A values. Kissinger plots were plotted to determine activation energies (E_a) and pre-exponential factors (A) of BNNT/epoxy resin nanocomposites with different BNNT contents as shown in Figure 40. Also, Table 10 lists the determined E_a and log$A$ values. Pre-exponential factor, A represents the rate factor which reactions occur in cure reactions[62]. The results suggest that as the content of BNNT increased, A values decreased as expected since the activation energies decreased.

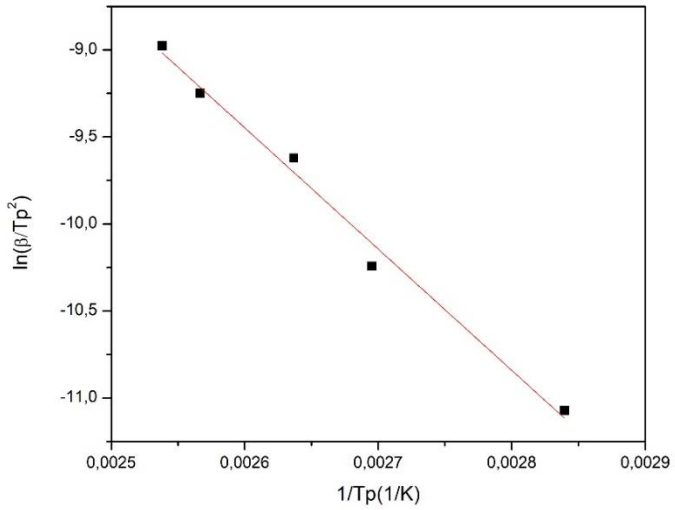

Figure 40:Example Kissinger plot to determine E_a and log*A* values for 0.5 wt% BNNT/epoxy resin nanocomposite

Table 10: E_a and log*A* Values Obtained by Kissinger Analysis

BNNT Content	**E_a (kJ/mol)**	**logA (1/s)**
0 wt%	61.35	8.06
0.25 wt%	56.86	7.46
0.50 wt%	57.94	7.6
0.75 wt%	51.46	6.76
1 wt%	54.35	7.14
2 wt%	55.71	7.32

3.5.1.4.3 Ozawa-Flynn-Wall Analyzes

Ozawa-Flynn-Wall (OFW) method was used to analyze variation in activation energies and pre-exponential factor, *A*' as a function of cure degree. E_a and *A'* values were calculated by plotting logβ against 1/T values for each degree of cure as shown in Figure 41. Figure 42 shows the obtained E_a and *A*' results for each nanocomposite. It is clear that the inclusion of BNNTs into

epoxy resins leads to decrease in both E_a and A'. BNNT weight fractions of 0.75 and 1 wt% resulted in a noticeable decrease which can be interpreted as fast curing whereas 0.25 and 0.5 wt% BNNTs were the least effective ones. They might not be enough to form an effective network in matrix due to their low quantity. Also, the decrease in activation energy of epoxy/amine systems was observed in literature [28, 63, 64]. It could be related to intermolecular crosslinking breaking which results in increasing chain mobility. In such a case, BNNTs act as obstacles in the system and prevent monomers to form larger molecules which results in higher mobility. Moreover, it could be due to the formation of hydroxyl groups during curing reactions.

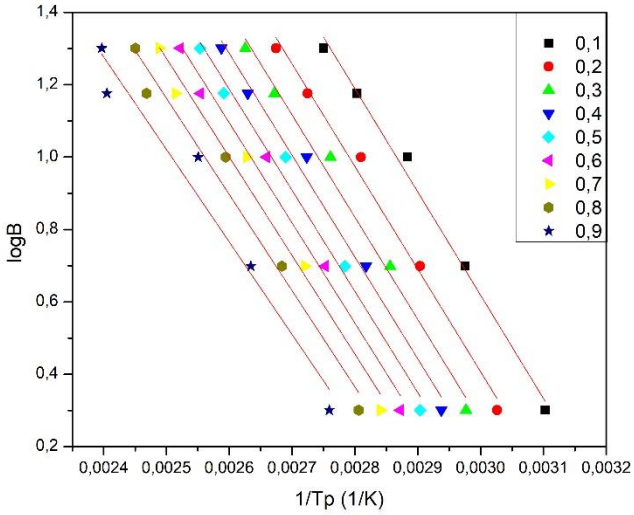

Figure 41: Example fit for Ozawa-Flynn-Wall method

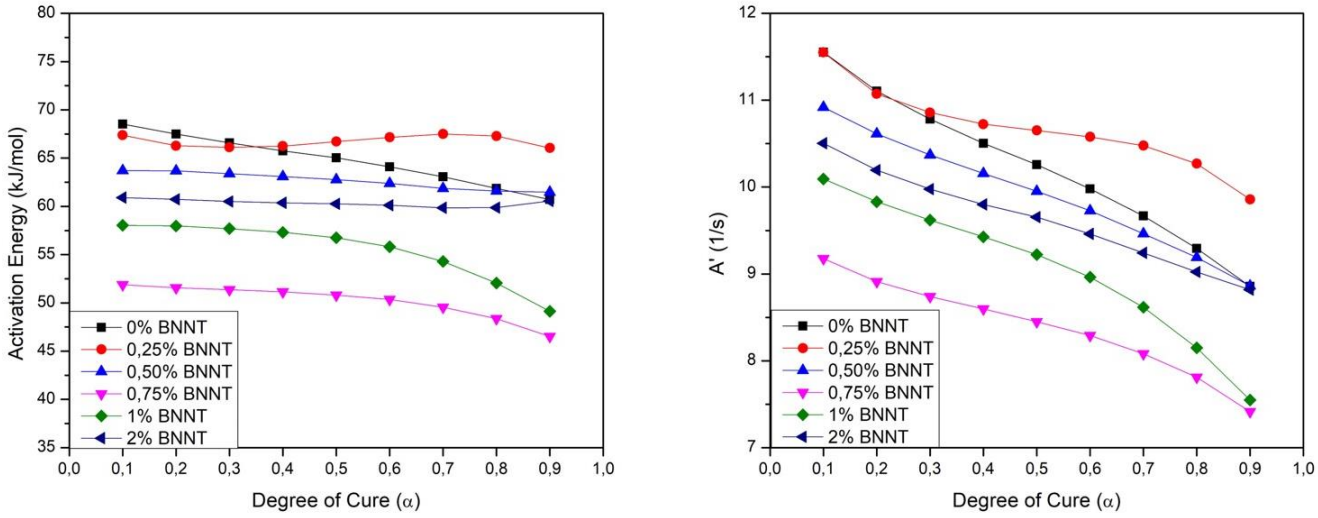

Figure 42: Activation energy and *A*' against degree of cure for BNNT/epoxy nanocomposites

3.5.1.5 Isothermal DSC Analyzes

In order to study isothermal curing behavior of epoxy resin system, three cure temperatures, 60˚C, 85˚C and 115˚C were chosen based on the dynamic scan of neat epoxy resin obtained by 10˚C/min heating rate. Figure 43 shows the isothermal cure cycles of BNNT/epoxy nanocomposites for cure temperature of 60˚C and obtained T_p, T_g, ΔH, ΔH_r values for different isothermal temperatures and times were listed in Tables 11, 12 and 13. The graphs show that enthalpy values decreased as expected when the time increased. The results suggest that curing reaction required more than 120 minutes for any BNNT/epoxy resin nanocomposites at isothermal cure temperature of 60 ˚C. On the other hand, cure reactions can be completed at nearly 60 minutes and 15 minutes at isothermal cure temperatures of 60 ˚C and 115 ˚C, respectively. In other words, curing time can be reduced when the isothermal cure temperature is increased as expected. On the contrary, T_g values increased when the isothermal waiting time increased. This can be attributed to formation of bigger crosslinked molecules due to curing which have reduced mobility.

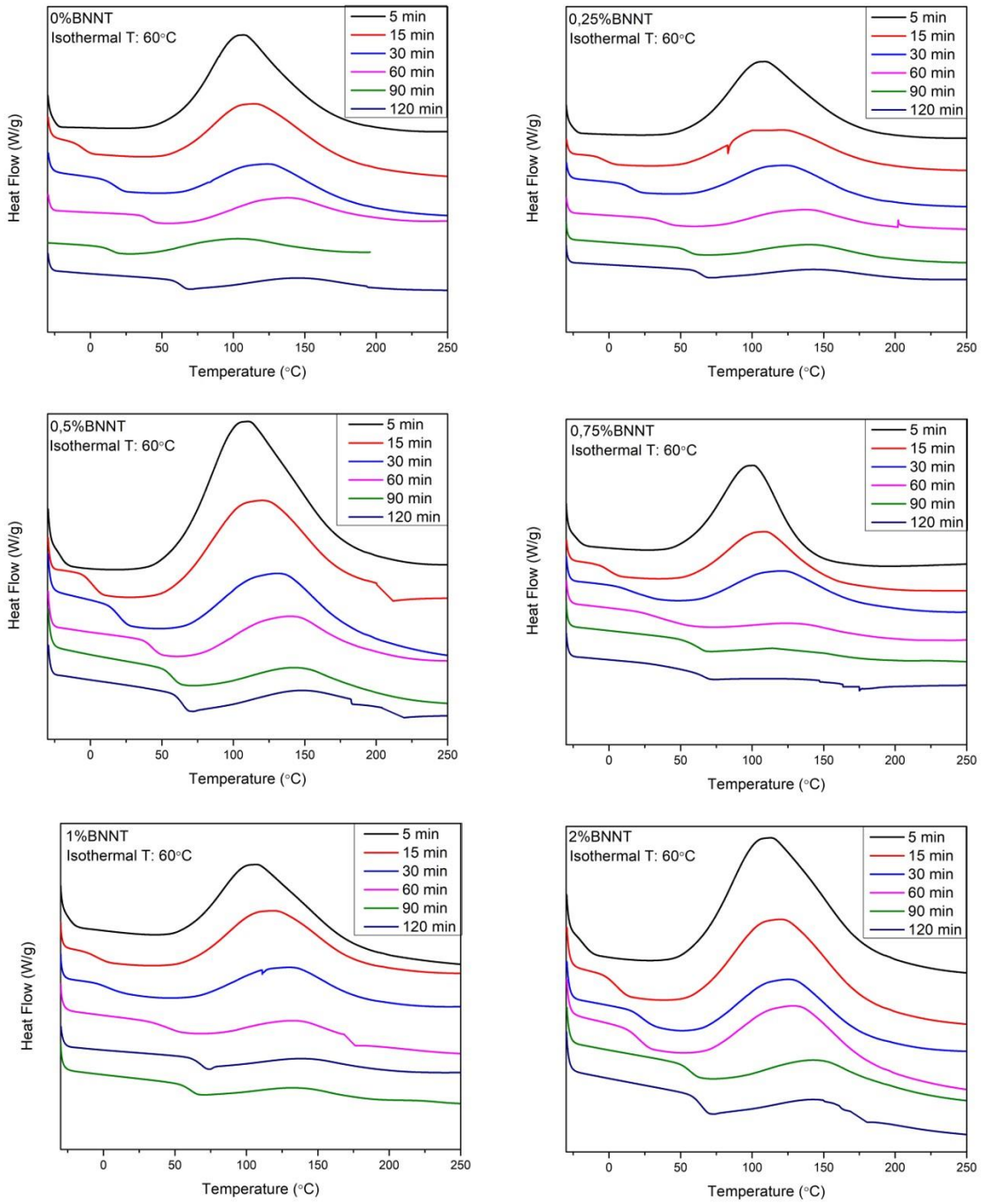

Figure 43:Isothermal DSC curves of the different BNNT content nanocomposites at isothermal cure temperature 60˚C for different waiting times

Table 11:Table of T_g, T_p, ΔH_r, ΔH and α Values of Different BNNT Content Nanocomposites at Isothermal Curing Temperature of 60˚C

Isothermal Temperature: 60 ˚C						
BNNT Content	**Time (min)**	**T_g (˚C)**	**T_p (˚C)**	**ΔH_r (J/g)**	**ΔH (J/g)**	**α**
0 wt%	5	-	107.86	376.6	464.4	0.19
	15	-5.43	115.97	262.2	464.4	0.44
	30	17.49	125.94	158.1	464.4	0.66
	60	39.97	137.04	114.3	464.4	0.75
	90	54.22	142.36	61.67	464.4	0.87
	120	63.24	144.17	47.16	464.4	0.90
0.25 wt%	5	-	108.94	356.4	413.4	0.14
	15	-3.13	121.22	222.1	413.4	0.46
	30	16.13	123.86	151.4	413.4	0.63
	60	38.03	137.12	82.13	413.4	0.80
	90	55.53	141.77	57.61	413.4	0.86
	120	64.27	143.94	50.47	413.4	0.88
0.50 wt%	5	-24.42	110.1	335.3	410.3	0.18
	15	1.84	120.73	254.3	410.3	0.38
	30	20.34	132.72	144.6	410.3	0.65
	60	43.16	140.48	100.4	410.3	0.76
	90	56.58	145	58	410.3	0.86
	120	64.97	1448.2	61	410.3	0.85
0.75 wt%	5	-25.58	100.74	244.8	321.8	0.24
	15	-1.59	109.1	145.2	321.8	0.55
	30	13.99	121.17	108.3	321.8	0.66

	60	36.52	129.59	20.9	321.8	0.94
	90	63.43	121.47	14.41	321.8	0.96
	120	66.6	136.94	11.57	321.8	0.96
1 wt%	5	-	107.94	300.1	409	0.27
	15	-5.23	119.16	228.5	409	0.44
	30	4.56	130.95	124.6	409	0.70
	60	45.38	136.3	64.4	409	0.84
	90	61.18	135.22	31.71	409	0.92
	120	68.84	141.03	33.2	409	0.92
2 wt%	5	-17.8	112.84	296.1	422.5	0.30
	15	6.57	121.03	210.7	422.5	0.50
	30	23.08	127.1	142	422.5	0.66
	60	19.8	131.7	143.5	422.5	0.66
	90	57.84	146.59	65.2	422.5	0.85
	120	64.18	145.96	34.48	422.5	0.92

Table 12:Table of T_g, T_p, ΔH_r, ΔH and α Values of Different BNNT Content Nanocomposites at Isothermal Curing Temperature of 85˚C

Isothermal Temperature: 85˚C						
BNNT Content	**Time (min)**	**T_g (˚C)**	**T_p (˚C)**	**ΔH_r (J/g)**	**ΔH (J/g)**	**α**
0 wt%	5	11.8	126.11	210.1	464.4	0.55
	15	45.5	139.42	94.64	464.4	0.80
	30	68.06	148.25	29.55	464.4	0.94
	60	85.85	149.76	12.39	464.4	0.97
	90				464.4	1.00

	120				464.4	1.00
0.25 wt%	5	15.81	129.81	182.2	413.4	0.56
	15	43.84	134.66	79.55	413.4	0.81
	30	65.31	146.6	35.77	413.4	0.91
	60	85.37	166.91	26.86	413.4	0.94
	90	93.26	145.95	18.42	413.4	0.96
	120				413.4	1.00
0.50 wt%	5	13.81	131.77	204.3	410.3	0.50
	15	44.37	142.47	85.11	410.3	0.79
	30	66.13	150.97	44.78	410.3	0.89
	60	83.28	156.03	9.071	410.3	0.98
	90				410.3	1.00
	120				410.3	1.00
0.75 wt%	5	23.64	113.45	49.8	321.8	0.85
	15	52.3	135.54	30.42	321.8	0.91
	30	56.33	146.55	17.33	321.8	0.95
	60	84.3	135.52	1.452	321.8	1.00
	90				321.8	1.00
	120				321.8	1.00
1 wt%	5	27.91	117.24	105.2	409	0.74
	15	45.94	137.21	43.89	409	0.89
	30	67.4	145.66	24	409	0.94
	60				409	1.00
	90				409	1.00
	120				409	1.00
2 wt%	5	17.19	127.35	144.8	422.5	0.66

	15	45.38	142.54	66.37	422.5	0.84
	30	67.89	125.19	41.28	422.5	0.90
	60	88.9	154.96	18.94	422.5	0.96
	90				422.5	1.00
	120				422.5	1.00

Table 13:Table of T_g, T_p, ΔH_r, ΔH and α Values of Different BNNT Content Nanocomposites at Isothermal Curing Temperature of 115˚C

Isothermal Temperature: 115˚C						
BNNT Content	**Time (min)**	**T_g (˚C)**	**T_p (˚C)**	**ΔH_r (J/g)**	**ΔH (J/g)**	**α**
0 wt%	5	63.07	146.67	49.24	464.4	0.89
	15	88.41	161.88	10.12	464.4	0.98
	30				464.4	1.00
	60	103.44	-	0	464.4	1.00
	90				464.4	1.00
	120				464.4	1.00
0.25 wt%	5	60.98	147.62	46.51	413.4	0.89
	15	88.68	162.35	8.615	413.4	0.98
	30	97.81	181.02	2.035	413.4	1.00
	60				413.4	1.00
	90				413.4	1.00
	120				413.4	1.00
0.50 wt%	5	63.23	148.69	50.19	410.3	0.88
	15	88.08	157.33	7.443	410.3	0.98
	30	97.94	196.62	1.091	410.3	1.00

	60	103.25	-	0	410.3	1.00
	90	113.35	-	0	410.3	1.00
	120	116.14	-	0	410.3	1.00
0.75 wt%	5	65.72	122.56	3.364	321.8	0.99
	15	78.18	153.44	0.86	321.8	1.00
	30				321.8	1.00
	60				321.8	1.00
	90				321.8	1.00
	120				321.8	1.00
1 wt%	5	64.41	142.15	20.32	409	0.95
	15	82.6	151.3	3.759	409	0.99
	30	97.44	-	0	409	1.00
	60				409	1.00
	90				409	1.00
	120				409	1.00
2 wt%	5	61.54	148.6	45.11	422.5	0.89
	15	88.83	156.63	11.78	422.5	0.97
	30	103.34	196.77	0.7474	422.5	1.00
	60	109.57	-	0	422.5	1.00
	90				422.5	1.00
	120				422.5	1.00

Figure 44 shows how the degree of cure values change with the addition of BNNTs for different isothermal temperatures and times. The results suggest that the addition of nanotubes accelerates the initial stage of curing. Degree of cure increased rapidly during the initial stages, then increased slowly and finally reached a plateau as expected. The fastest curing reactions occurred at 0.75 wt% BNNT content and was followed by the 1 wt% BNNT content for all isothermal temperatures.

It can be attributed to both amount and dispersion of nanotubes. It was observed that the 0.75 wt% BNNT content had a good dispersion with local agglomerations while 1 wt% BNNT content had homogenous agglomerations (see Figures 37 and 38). Also, 2 wt% BNNT content accelerated the initial stage of curing, but it was lower than 0.75 wt% and 1 wt% BNNT contents which can be attributed to the agglomerations of nanotubes. When nanotubes form agglomerations, their surface area decrease, and they cannot interact with the polymer as they interact with each other. Also, they can cause a physical hindrance to the mobility of epoxy monomers. On the other hand, even though, the dispersions of lower BNNT contents were homogenous, they only had slight effects on the curing reactions and were not very effective on curing mechanism. The amount of nanotubes for 0.25 wt% and 0.5 wt% BNNT content may not be enough to form an effective network inside the matrix.

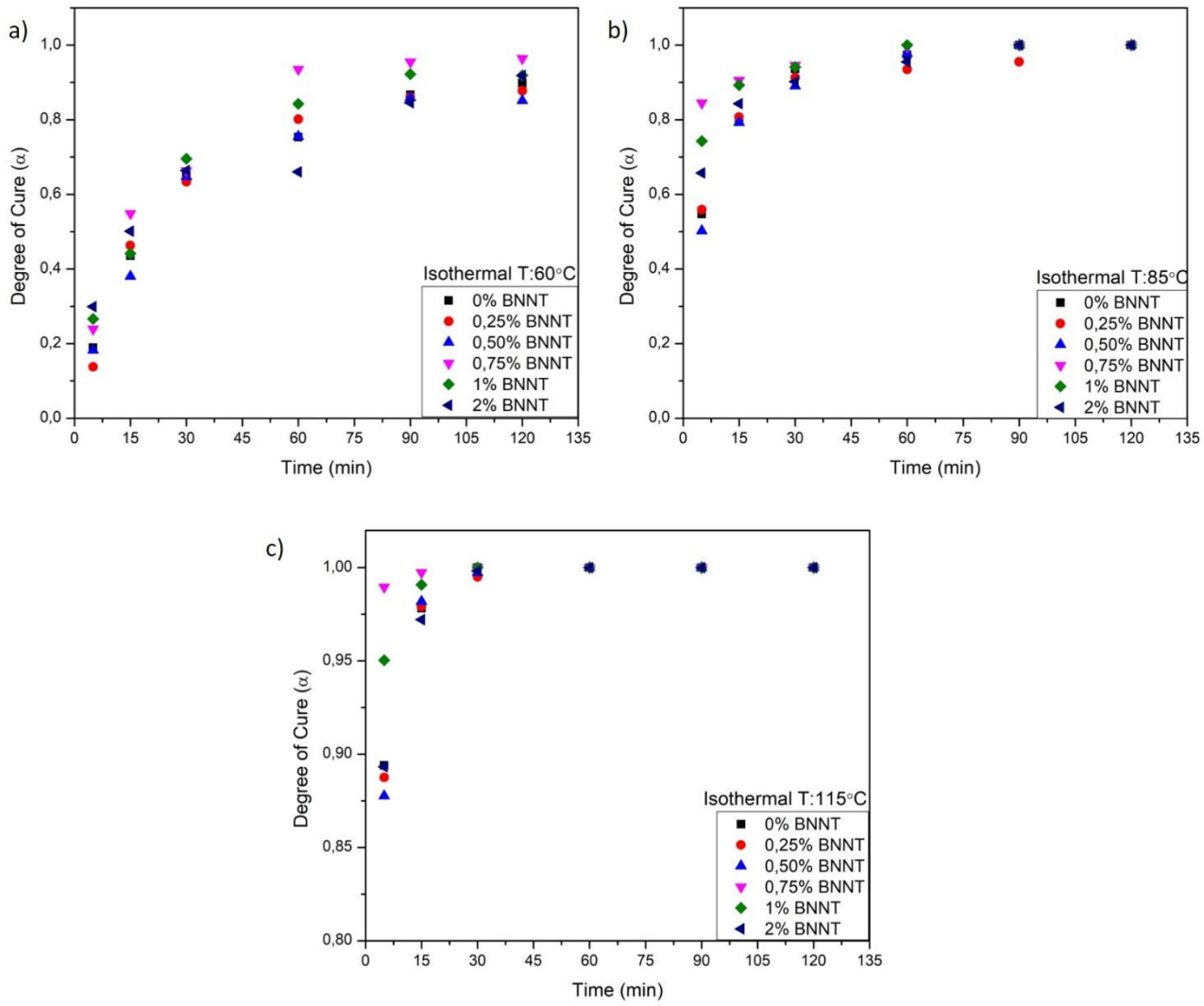

Figure 44:Degree of cure against time for isothermal cure temperatures a)60˚C b)85˚C and c)115˚C

3.5.1.6 Kinetic Model Fitting

Degree of cure against temperature plots are important indicators for kinetic models. As seen in Figure 45, the trend in conversion against temperature were sigmoidal for each system, independent from the BNNT content. The sigmoidal shape in plots indicates that the cure reaction in BNNT/epoxy resin system was governed by autocatalytic reaction mechanism. The sigmoidal curves shifted to higher temperatures with increasing heating rates. It was attributed to increasing

amount of time due to slower heating rates which systems can react in lower temperatures and therefore complete cure reactions in lower temperatures (see Chapter 3.5.4.1).

It was observed that the addition of BNNTs into epoxy resin did not change the sigmoidal behavior as seen in Figure 45. Thus, it can be said that the BNNTs do not change the autocatalytic cure mechanism of epoxy resin. Moreover, degree of cure against temperature for a constant heating rate of 2˚C/min was plotted in Figure 46 for further examination of the effects of BNNTs. It was observed that the addition of BNNTs accelerated the initial stage of curing process. They acted as catalysts to initiate curing at lower temperatures. 0.75 wt% BNNT content nanocomposite achieved higher degrees of curing at lower temperatures and was followed by the 1 wt% which is another indication for the importance of dispersion. Optical microscopy image of 0.75 wt% BNNT content shows good dispersion while 1 wt% also exhibited agglomerated but homogeneous dispersions inside epoxy resin matrix. On the other hand, results for 0.25, 0.5 and 2 wt% BNNT contents were close and not very effective compared to 0 wt%. This behavior can be explained by two main reasons: Firstly, quantity of nanotubes was not sufficient to affect the overall system for the first two cases. Secondly, big agglomerations in the latter case hindered the possible effects. Thus, it can be concluded that well dispersed BNNTs accelerate the cure reaction of epoxy resins especially at the initial stage and lower the required cure temperature. Consequently, they decrease the time required for the complete curing.

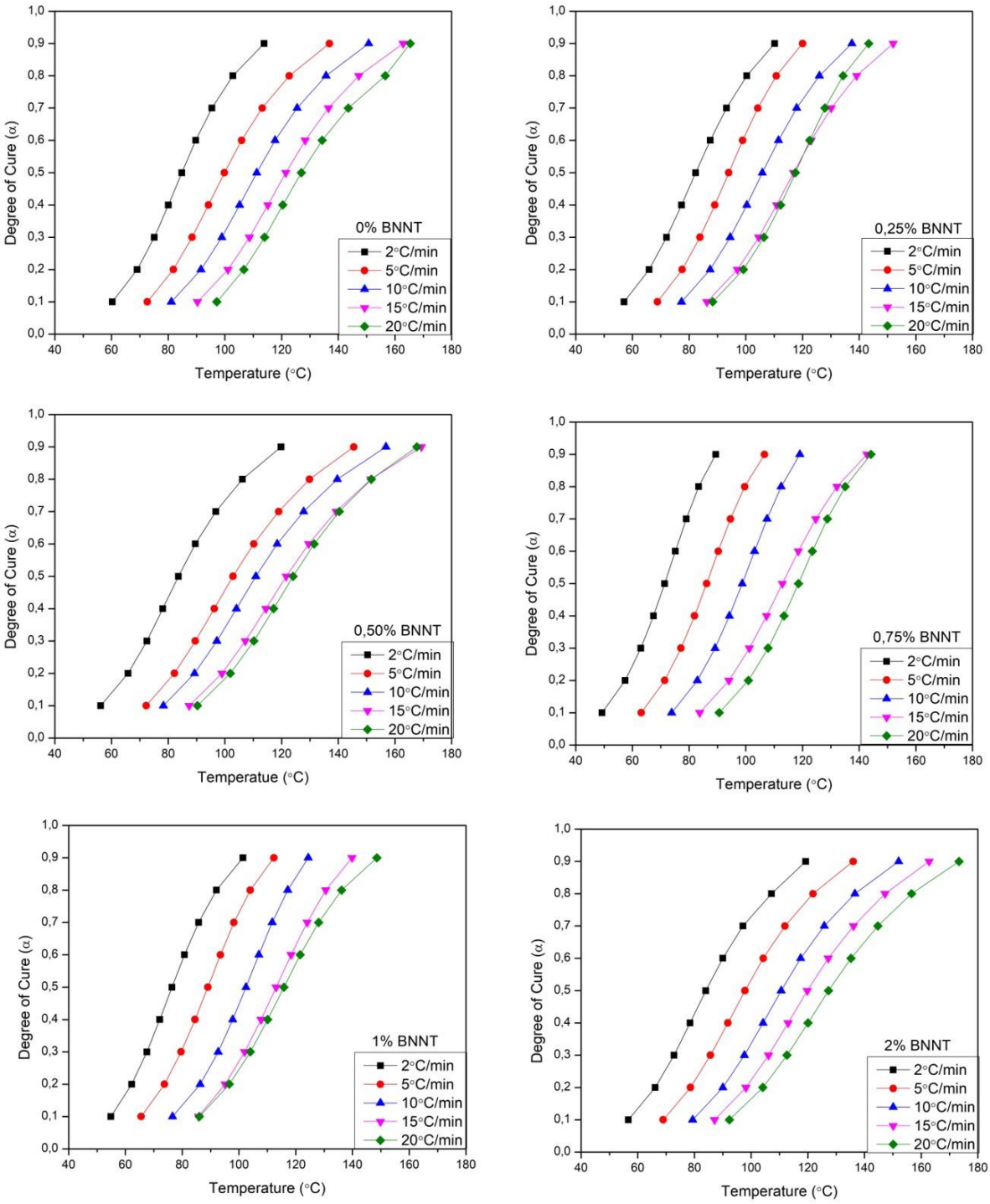

Figure 45: Degree of cure against temperature plots for different BNNT content nanocomposites

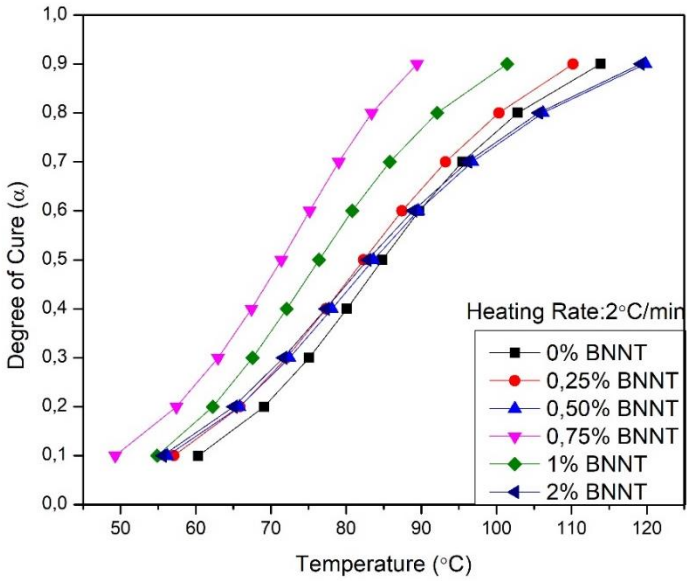

Figure 46:Degree of cure against temperature plot of different BNNT content nanocomposites (Heating rate:2˚C/min)

Autocatalytic kinetic model assumes that the degree of cure at the peak temperature supposed to be constant independent from the heating rate [25]. Table 14 shows the degree of cure values for peak temperatures for different BNNT content nanocomposites.

Table 14: Degree of Cure Values at Peak Temperature of Exotherm

0 wt% BNNT	**Tp (˚C)**	**α**	**0.25 wt% BNNT**	**Tp (˚C)**	**α**	**0.50 wt% BNNT**	**Tp (˚C)**	**α**
2˚C/min	84.04	0.45	**2˚C/min**	80.48	0.46	**2˚C/min**	79.17	0.42
5˚C/min	98.67	0.44	**5˚C/min**	96.10	0.54	**5˚C/min**	98.03	0.42
10˚C/min	107.88	0.45	**10˚C/min**	106.27	0.51	**10˚C/min**	106.26	0.43
15˚C/min	120.44	0.49	**15˚C/min**	116.20	f0.50	**15˚C/min**	116.64	0.43
20˚C/min	122.84	0.47	**20˚C/min**	124.17	0.63	**20˚C/min**	120.99	0.45
0.75 wt% BNNT	**Tp (˚C)**	**α**	**1 wt% BNNT**	**Tp (˚C)**	**α**	**2 wt% BNNT**	**Tp (˚C)**	**α**
2˚C/min	73.90	0.56	**2˚C/min**	75.55	0.52	**2˚C/min**	78.37	0.42
5˚C/min	89.31	0.57	**5˚C/min**	97.24	0.49	**5˚C/min**	94.92	0.45
10˚C/min	103.12	0.60	**10˚C/min**	105.51	0.45	**10˚C/min**	105.75	0.46
15˚C/min	113.85	0.52	**15˚C/min**	114.11	0.52	**15˚C/min**	114.25	0.45
20˚C/min	118.93	0.51	**20˚C/min**	119.33	0.53	**20˚C/min**	122.45	0.44

Dynamic DSC measurements were used to determine the governing model for the cure reaction of epoxy resin system. After the model was determined as an autocatalytic reaction model, isothermal DSC measurements were used to find reaction orders, m and n. Table 15 lists the reaction orders m, n and R^2 values which were determined by applying linear regression method (Isothermal temperature 115˚C was not included since it only had two data points) and comparison plots of experimental data against model fitted data was shown in Figure 47.

Table 15: Values of Reaction Orders, m, n and R^2

Isothermal Temperature 60˚C	**m**	**n**	**R^2**	**Isothermal Temperature 85˚C**	**m**	**n**	**R^2**
0 wt% BNNT	1.95	4.67	0.97	**0 wt %BNNT**	5.54	3.02	0.98
0.25 wt% BNNT	2.30	6.58	0.98	**0.25 wt% BNNT**	5.76	3.07	0.99
0.50 wt% BNNT	2.62	6.32	0.86	**0.50 wt% BNNT**	5.04	3.18	0.99
0.75 wt% BNNT	3.93	7.02	0.97	**0.75 wt% BNNT**	15.06	2.66	0.98
1 wt% BNNT	3.96	6.29	0,82	**1 wt% BNNT**	9.71	2.64	0.99
2 wt% BNNT	3.54	6.07	0.95	**2 wt% BNNT**	7.16	3.00	0.98

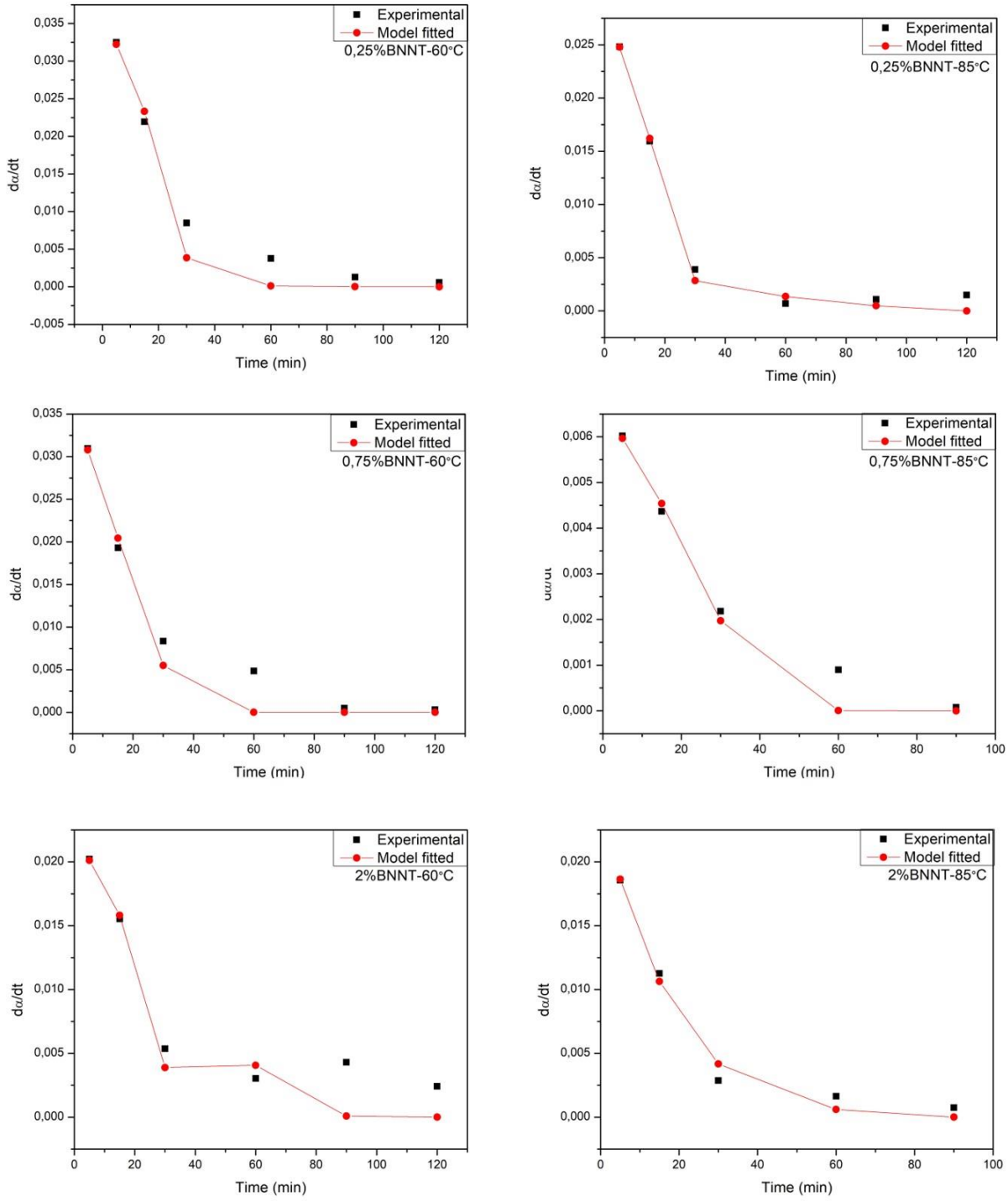

Figure 47: Plots of experimental dα/dt against fitted models

3.6 Conclusions

The effects of BNNT addition into epoxy resin system was investigated in this chapter. The cure behaviors of different BNNT content/epoxy resins were characterized by using dynamic and isothermal DSC measurements. The dynamic DSC measurements showed that peak temperature of exothermic cure reaction shifted to lower temperatures with the addition of BNNTs which indicates that BNNTs had an accelerating effect at the initial stage of curing. Activation energy values obtained by Kissinger and Ozawa-Flynn-Wall methods showed a reasonable agreement except for 0.25 wt% BNNT content. Isothermal cure analysis of the systems indicated that higher isothermal cure temperatures decreased the time to complete cure reactions. Moreover, addition of BNNTs decreased the time required to complete curing with respect to neat epoxy. Addition to these, accelerating effects of BNNTs were observed in isothermal measurements as well. Degree of cure increased rapidly during the initial stage of curing and completed in lower temperatures compared to neat epoxy. The fastest curing reactions occurred at 0.75 wt% BNNT content and were followed by the 1wt% BNNT content for all isothermal temperatures which can be attributed to amount and the dispersion of nanotubes. It can be concluded that BNNT/epoxy resin systems possess a fast curing feature.

Also, kinetic model fitting was performed, and kinetic parameters were calculated by linear regression as a part of the cure study. The results indicated that the governing curing mechanism was autocatalytic model and addition of BNNTs into epoxy resin did not change curing mechanism of the system.

Moreover, possible cure recipes for BNNT/epoxy resin nanocomposites were derived based on the observed isothermal cure behaviors as listed in Table 18.

Table 16:Curing Recipes for BNNT/Epoxy Nanocomposites

Curing Recipe	BNNT Content (%)	Dynamic Heating Rate (°C/min)	Isothermal Temperature (°C)	Isothermal Waiting Time (min)	Achieved Degree of Cure (α)	Estimated Time Required for Full Cure (t) (min)
R1	0	10	60	120	0,89	t>120
	0.25	10	60	120	0,88	t>120
	0.50	10	60	120	0,85	t>120
	0.75	10	60	120	0,96	t>120
	1	10	60	120	0,92	t>120
	2	10	60	120	0,92	t>120
R2	0	10	85	60	0,97	90>t>60
	0.25	10	85	90	0,96	120>t>90
	0.50	10	85	60	0,98	90>t>60
	0.75	10	85	60	~1	t~60
	1	10	85	30	0,94	60>t>30
	2	10	85	60	0,95	90>t>60
R3	0	10	115	15	0,98	30>t>15
	0.25	10	115	30	~1	30>t>15
	0.50	10	115	15	0,98	30>t>15
	0.75	10	115	15	~1	15>t>5
	1	10	115	15	0,99	30>t>15
	2	10	115	15	0,97	30>t>15

4 Chapter 4

4.1 General Conclusions

The thesis presented here was organized as two parts: In the first part of to study, a full factorial experimental design was conducted to analyze the effects of reaction temperature, heating rate and reactive gas flow rate on diameter, aspect ratio and wafer coverage of BNNTs. Empirical models were developed to understand system's behavior. Experimental values and predicted results from the developed models showed a reasonable agreement for each response. A multiple response surface optimization study was performed to determine a compromised solution which satisfies each response as possible. The optimum conditions for maximum aspect ratio and maximum coverage was found as 1190˚C reaction temperature, 5˚C/min heating rate and 200 ml/min reactive gas flow rate.

In the second part of the study, effects of BNNT addition into epoxy resin system on curing was investigated. The cure behavior at different BNNT loading was characterized by using dynamic and isothermal DSC measurements. The dynamic DSC measurements showed that peak temperature of exothermic cure reaction shifted to lower temperatures with the addition of BNNTs which indicates that BNNTs have an accelerating effect at the initial stage of curing. Activation energy values obtained by Kissinger and Ozawa-Flynn-Wall methods showed a reasonable agreement except for 0.25 wt % BNNT content. Isothermal cure analysis of the systems confirmed that higher isothermal cure temperatures decreased the time to complete cure reactions. Moreover, addition of BNNTs decreased time required for complete curing with respect to neat epoxy. Accelerating effects of BNNTs were observed in isothermal measurements as well and degree of cure increased rapidly during the initial stage of curing and completed in lower temperatures compared to 0 wt% BNNT content. The fastest curing reactions occurred at 0.75 wt% BNNT content and were followed by the 1 wt% BNNT content for all isothermal temperatures which can be attributed to the balance of amount and the dispersion of the nanotubes. Thus, it can be concluded that BNNT/epoxy resin systems possess a fast curing feature. Moreover, possible cure recipes for BNNT/epoxy resin nanocomposites were derived based on the observed isothermal cure behaviors.

Moreover, kinetic model fitting was performed, and associated parameters were calculated by linear regression as a part of the cure study. The results indicate that the governing curing mechanism was correlated by autocatalytic model and addition of BNNTs into epoxy resin did not change curing mechanism of the system.

5 References

1. Golberg, D., et al., *Boron Nitride Nanotubes.* Advanced Materials, 2007. **19**(18): p. 2413-2432.
2. Pakdel, A., et al., *A comprehensive analysis of the CVD growth of boron nitride nanotubes.* Nanotechnology, 2012. **23**(21): p. 215601.
3. Nasreen G. Chopra, R.J.L., K. Cherrey, Vincent H. Crespi, Marvin L. Cohen, Steven G. Louie, A. Zettl1, *Boron Nitride Nanotubes.* Science, 1995. **269**(5226): p. 966-967.
4. Dmitri Golberg, et al., *Boron Nitride Nanotubes and Nanosheets.* ACS Nano, 2010. **4**(6): p. 2979-2993.
5. Lee, C.H., et al., *Patterned Growth of Boron Nitride Nanotubes by Catalytic Chemical Vapor Deposition.* Chemistry of Materials, 2010. **22**(5): p. 1782-1787.
6. Zhi, C., et al., *Effective precursor for high yield synthesis of pure BN nanotubes.* Solid State Communications, 2005. **135**(1-2): p. 67-70.
7. Rubio, A., J.L. Corkill, and M.L. Cohen, *Theory of graphitic boron nitride nanotubes.* Physical Review B, 1994. **49**(7): p. 5081-5084.
8. X. Blase, A.R., S. G. Louie, M.L. Cohen, *Stability and band gap canstancy of boron nitride nanotubes.* Europhysics Letters, 1994. **28**(5): p. 335-340.
9. Wang, J., C.H. Lee, and Y.K. Yap, *Recent advancements in boron nitride nanotubes.* Nanoscale, 2010. **2**(10): p. 2028-34.
10. Terrones, M., et al., *Pure and doped boron nitride nanotubes.* Materials Today, 2007. **10**(5): p. 30-38.
11. D. Golberg, Y.B., M. Eremets, K. Takemura, K. Kurashima, and H. Yusa, *Nanotubes in boron nitride laser heated at high pressure.* Appl. Phys. Lett., 1996. **69**(14).
12. Tang, C., et al., *A novel precursor for synthesis of pure boron nitride nanotubesElectronic supplementary information (ESI) available: (a) experimental apparatus and details; (b) Fig. S2, XRD pattern of BN nanotubes; (c) XRD pattern of the product formed by dispersive Mg at the surface of the graphite susceptor; (d) Fig. S4, EELS spectrum of BN nanotubes; (e) Fig. S5, selected-area electron diffraction; (f) Fig. S6, EDS analysis of open tip. See* http://www.rsc.org/suppdata/cc/b2/b202177c. Chemical Communications, 2002(12): p. 1290-1291.

13. R. Ma, Y. Bando, and T. Sato, *CVD synthesis of boron nitride nanotubes without metal catalysts.* Chemical Physics Letters, 2001(337): p. 61-64.
14. Weiqiang Han, Y.B., Keiji Kurashima, and Tadao Sato, *Synthesis of boron nitride nanotubes from carbon nanotubes by a substitution reaction.* Applied physics letters, 1998. **73**: p. 3085.
15. Ying Chen, L.T.C., John Fitz Gerald, James S. Williams, *A solid-state process for formation of boron nitride nanotubes.* Applied physics letters, 1999. **74**: p. 2960-2962.
16. Lee, C.H., et al., *Effective growth of boron nitride nanotubes by thermal chemical vapor deposition.* Nanotechnology, 2008. **19**(45): p. 455605.
17. Singhal, S.K., et al., *Synthesis of boron nitride nanotubes by an oxide-assisted chemical method.* Journal of Nanoparticle Research, 2009. **12**(7): p. 2405-2413.
18. Montgomery, D.C., *Design and Analysis of Experiments*. Eigth edition ed. 2013: John Wiley & Sons, Inc.
19. Bezerra, M.A., et al., *Response surface methodology (RSM) as a tool for optimization in analytical chemistry.* Talanta, 2008. **76**(5): p. 965-77.
20. Liu, W.-W., et al., *Optimisation of reaction conditions for the synthesis of single-walled carbon nanotubes using response surface methodology.* The Canadian Journal of Chemical Engineering, 2012. **90**(2): p. 489-505.
21. Porro, S., et al., *Optimization of a thermal-CVD system for carbon nanotube growth.* Physica E: Low-dimensional Systems and Nanostructures, 2007. **37**(1-2): p. 16-20.
22. Kuo, C.-S., et al., *Diameter control of multiwalled carbon nanotubes using experimental strategies.* Carbon, 2005. **43**(13): p. 2760-2768.
23. Kukovecz, Á., et al., *Optimization of CCVD synthesis conditions for single-wall carbon nanotubes by statistical design of experiments (DoE).* Carbon, 2005. **43**(14): p. 2842-2849.
24. See, C.H., et al., *Multi-parameter optimisation of carbon nanotube synthesis in fluidised-beds.* Chemical Engineering Science, 2009. **64**(16): p. 3614-3621.
25. Chandran, M.S., et al., *Cure Kinetics and Activation Energy Studies of Modified Bismaleimide Resins.* ISRN Polymer Science, 2012. **2012**: p. 1-8.
26. Du, S., et al., *Cure kinetics of epoxy resin used for advanced composites.* Polymer International, 2004. **53**(9): p. 1343-1347.

27. Joseph D. Menczel, R.B.P., *Thermal Analysis of Polymers Fundamentals and Applications*. 2009, Hoboken, New Jersey: John Wiley & Sons, Inc. .
28. Thanki, J.D. and P.H. Parsania, *Dynamic DSC curing kinetics and thermogravimetric study of epoxy resin of 9,9'-bis(4-hydroxyphenyl)anthrone-10.* Journal of Thermal Analysis and Calorimetry, 2017. **130**(3): p. 2145-2156.
29. Wen-Yi, C., W. Yez-Zen, and C. Feng-Chih, *Study on curing kinetics and curing mechanism of epoxy resin based on diglycidyl ether of bisphenol a and melamine phosphate.* Journal of Applied Polymer Science, 2004. **92**(2): p. 892-900.
30. Zhao, S.F., et al., *Curing kinetics, mechanism and chemorheological behavior of methanol etherified amino/novolac epoxy systems.* Express Polymer Letters, 2014. **8**(2): p. 95-106.
31. Saeb, M.R., et al., *Cure kinetics of epoxy nanocomposites affected by MWCNTs functionalization: a review.* ScientificWorldJournal, 2013. **2013**: p. 703708.
32. Xie, H., et al., *Cure kinetics of carbon nanotube/tetrafunctional epoxy nanocomposites by isothermal differential scanning calorimetry.* Journal of Polymer Science Part B: Polymer Physics, 2004. **42**(20): p. 3701-3712.
33. Zhou, T., et al., *Influence of multi-walled carbon nanotubes on the cure behavior of epoxy-imidazole system.* Carbon, 2009. **47**(4): p. 1112-1118.
34. Rafique, I., A. Kausar, and B. Muhammad, *Epoxy Resin Composite Reinforced with Carbon Fiber and Inorganic Filler: Overview on Preparation and Properties.* Polymer-Plastics Technology and Engineering, 2016. **55**(15): p. 1653-1672.
35. Iijima, S., *Helical microtubules of graphitic carbon.* Nature, 1991. **354**(6348): p. 56-58.
36. D. Puglia, L.V., J. M. Kenny, *Analysis of the Cure Reaction of Carbon Nanotubes/Epoxy Resin Composites Through Thermal Analysis and Raman Spectroscopy.* journal of applied Polymer Science, 2003. **88**: p. 452-458.
37. Lee, D., et al., *Enhanced mechanical properties of epoxy nanocomposites by mixing noncovalently functionalized boron nitride nanoflakes.* Small, 2013. **9**(15): p. 2602-10.
38. Ciecierska, E., et al., *The effect of carbon nanotubes on epoxy matrix nanocomposites.* Journal of Thermal Analysis and Calorimetry, 2012. **111**(2): p. 1019-1024.
39. Chen, X., et al., *Mechanical strength of boron nitride nanotube-polymer interfaces.* Applied Physics Letters, 2015. **107**(25): p. 253105.

40. Zhi, C., et al., *Towards Thermoconductive, Electrically Insulating Polymeric Composites with Boron Nitride Nanotubes as Fillers.* Advanced Functional Materials, 2009. **19**(12): p. 1857-1862.
41. Ashrafi, B., et al., *Multifunctional fiber reinforced polymer composites using carbon and boron nitride nanotubes.* Acta Astronautica, 2017. **141**: p. 57-63.
42. Candioti, L.V., et al., *Experimental design and multiple response optimization. Using the desirability function in analytical methods development.* Talanta, 2014. **124**: p. 123-38.
43. Zhu, G., et al., *In situ growth behavior of boron nitride nanotubes on the surface of silicon carbide fibers as hierarchical reinforcements.* RSC Advances, 2016. **6**(17): p. 14112-14119.
44. Ahmad, P., et al., *Synthesis of boron nitride nanotubes via chemical vapour deposition: a comprehensive review.* RSC Advances, 2015. **5**(44): p. 35116-35137.
45. Baysal, M., et al., *Catalytic synthesis of boron nitride nanotubes at low temperatures.* Nanoscale, 2018. **10**(10): p. 4658-4662.
46. R.Arenal, et al., *Raman Spectroscopy of Single-Wall Boron Nitride Nanotubes.* NANO Letters, 2006. **6**(8): p. 1812-1816.
47. M. Zdrajek, W.G., C. Jastrzebski, T. Melin, A. Huczko, *Studies of multiwall carbon nanotubes using Raman spectroscopy and atomic force microscopy.* Solid State Phenomena 2004. **99**(265).
48. Frans W. Langkilde, J.S.b., Lija Tekenbergs-Hjelte , Jonni Mrak *Quantitative FT-Raman analysis of two crystal forms of a pharmaceutical compound.* Journal of Pharmaceutical and Biomedical Analysis, 1996. **15**: p. 687-696.
49. C. Moorea, T.S.P., B. Kennedy, K. Berwickc, I.I. Shaganovd, and R.A. Moorea, *Study of structure and quality of different silicon oxides using FTIR and Raman microscopy.* Proceedings of SPIE, 2002.
50. Jarrah, N.A., *Studying the influence of process parameters on the catalytic carbon nanofibers formation using factorial design.* Chemical Engineering Journal, 2009. **151**(1-3): p. 367-371.
51. Yördem, O.S., M. Papila, and Y.Z. Menceloğlu, *Effects of electrospinning parameters on polyacrylonitrile nanofiber diameter: An investigation by response surface methodology.* Materials & Design, 2008. **29**(1): p. 34-44.

52. Yan, H., et al., *Enhanced thermal–mechanical properties of polymer composites with hybrid boron nitride nanofillers.* Applied Physics A, 2013. **114**(2): p. 331-337.
53. Stuart, B.H., *Polymer Analysis*. Analytical Techniques in the Sicence (AnTS), ed. D.J. Ando. 2002, England: John Wiley&Sons, Ltd.
54. Ehlers, J.-E., et al., *Theoretical Study on Mechanisms of the Epoxy−Amine Curing Reaction.* Macromolecules, 2007. **40**(12): p. 4370-4377.
55. Ma, P.-C., et al., *Dispersion and functionalization of carbon nanotubes for polymer-based nanocomposites: A review.* Composites Part A: Applied Science and Manufacturing, 2010. **41**(10): p. 1345-1367.
56. Pizzutto, C.E., et al., *Study of epoxy/CNT nanocomposites prepared via dispersion in the hardener.* Materials Research, 2011. **14**(2): p. 256-263.
57. Bilge, K., et al., *Stabilized electrospinning of heat stimuli/in situ crosslinkable nanofibers and their self-same nanocomposites.* Journal of Applied Polymer Science, 2016. **133**(43).
58. Wang, J., C.H. Lee, and Y.K. Yap, *Recent advancements in boron nitride nanotubes.* Nanoscale, 2010. **2**(10): p. 2028-2034.
59. B., N.M., et al., *The thermal degradation of some epoxy resins.* Journal of Polymer Science, 1962. **56**(164): p. 383-389.
60. Golberg, D., et al., *Boron Nitride Nanotubes and Nanosheets.* ACS Nano, 2010. **4**(6): p. 2979-2993.
61. Nonahal, M., et al., *Epoxy/PAMAM dendrimer-modified graphene oxide nanocomposite coatings: Nonisothermal cure kinetics study.* Progress in Organic Coatings, 2018. **114**: p. 233-243.
62. Peter Atkins, J.D.P., *Atkins' Physical Chemistry*. 9th ed. 2010: Oxford University Press.
63. Lakho, D.A., et al., *Study of the Curing Kinetics toward Development of Fast-Curing Epoxy Resins.* Polymer-Plastics Technology and Engineering, 2016. **56**(2): p. 161-170.
64. Patel, A., et al., *Curing Kinetics of Biobased Epoxies for Tailored Applications.* Macromolecules, 2016. **49**(15): p. 5315-5324.